Experimental Thermal and Fluid Science 172 (2026) 111626

Contents lists available at ScienceDirect

Experimental Thermal and Fluid Science

journal homepage: www.elsevier.com/locate/etfs

Nanofluids mixed convection, heat transfer characteristics and effects of volume concentrations in the thermally developing region

Ibrahim Umar Ibrahim [a,b,*], Mohsen Sharifpur [a,c,d,*], Josua P. Meyer [a,e]

[a] Department of Mechanical and Aeronautical Engineering, University of Pretoria, Pretoria 0002, South Africa
[b] Department of Mechanical Engineering, Ahmadu Bello University, Zaria, Kaduna State, Nigeria
[c] School of Mechanical, Industrial and Aeronautical Engineering, University of the Witwatersrand, Private Bag 3, Wits 2050, South Africa
[d] Department of Medical Research, China Medical University Hospital, China Medical University, Taichung, Taiwan
[e] Department of Mechanical and Mechatronic Engineering, Stellenbosch University, Stellenbosch, South Africa

ARTICLE INFO

Keywords:
Mixed convection
Transition boundaries
Thermal entrance length
Thermally developing flow

ABSTRACT

The vast majority of research on nanofluids only focuses on the heat transfer enhancement and pressure drop characteristics of these fluids. But apart from that, there are other intricate and complex phenomena that are very critical to the understanding of these fluid's characteristics. The effects of free convection, entrance effects, and the influence of volume concentration on boundary conditions (i.e., laminar start and end, transition and turbulence) were often neglected. This limits our knowledge of these fluids. These phenomena were critical to understanding and fully utilising nanofluid potentials. Therefore, this research experimentally investigated the force and mixed convection of Al_2O_3- MWCNT/water hybrid nanofluids. Three different concentrations of 0.30, 0.20, and 0.10 were prepared using the two-step method. Results show that an increase in volume concentration significantly affects nanofluid transition boundaries. Because critical Reynolds numbers for all the volume concentrations varied significantly, results show that critical Reynolds numbers of 0.3, 0.2 and 0.1 vol concentrations are $Re_{cr.} = 2140$, 2200, and 2330, respectively. Thermal entrance influences were found to decrease with the increase in volume concentration. Mixed convection effects were increased with a decrease in volume concentration. Results also revealed that the Nusselt number of 0.3 vol concentration at $Re = 1000$ was enhanced by about 50 % within the thermal entrance length. In contrast, it was enhanced by about 48.84 % due to mixed convection. It was concluded that heat transfer enhancement was much better due to thermal entrance effects than with mixed convection. Also, the fluid viscosity depends on transition region boundaries, thermal entrance effects, and mixed convection heat transfer characteristics. Also, their characteristics often differ at different axial positions.

1. Introduction

Despite the emergence of hybrid nanofluids with better thermophysical properties and improved forced convective heat transfer characteristics. Experimental research on these fluid's mixed convection heat transfer characteristics is very limited. These fluids have distinctive and very peculiar properties compared to other single or mono-nanofluids (i.e., Nanofluids with single nanoparticles) and conventional fluids (e.g., water). This is due to the two different and distinctive metal- or metal-based oxide nanoparticles dispersed in the base fluids. The possibility of having these dispersed nanoparticles in different percentage weight compositions gives more flexibility in enhancing their thermal and heat transfer characteristics. Properties such as viscosity, heat capacity, fluid density and thermal conductivity were all affected or varied when the weight composition of the particles in the hybrid nanofluid varied [1]. The most important properties that significantly impact hybrid nanofluid heat transfer are viscosity, thermal conductivity, and density [1,2]. Research on nanofluid thermo-physical characteristics shows that their viscosity varies with temperature, and its influence on heat transfer characteristics proved very significant [2]. The impact of viscosity variation on the nanofluid's heat transfer characteristics was expected to be more significant with mixed convection.

Findings from the research work of Buongiorno et al. [3] revealed that adding metallic nanoparticles to the base fluid may influence the secondary flow. Because there is a tendency to increase the irregular and random nanoparticle motion, which may increase the secondary flow strength. An increase in secondary flow significance enhances heat

* Corresponding authors at: Department of Mechanical and Aeronautical Engineering, University of Pretoria, Pretoria 0002, South Africa.
E-mail addresses: ibrahimu334@gmail.com (I. Umar Ibrahim), mohsen.sharifpur@up.ac.za (M. Sharifpur).

https://doi.org/10.1016/j.expthermflusci.2025.111626
Received 20 August 2025; Received in revised form 1 October 2025; Accepted 7 October 2025
Available online 21 October 2025

Nomenclature

A	Constants
A_s	Surface Area [m^2]
C_{bf}	Specific heat capacity of base [J/kgK]
C_{hnf}	Specific heat capacity of Hybrid [J/kgK]
c_p	Specific heat capacity of Particles [J/kgK]
D_{si}	Internal Tube diameter [m]
D_{so}	Outer Tube Diameter [m]
g	Acceleration due to gravity
Gr	Grashof Number
Gz	Graetz Number
$h(x)$	Local Heat transfer coefficient [W/m^2K]
h_{avg}	Average Coefficient of Heat Transfer [W/m^2K]
I	Current [A]
J	Colburn J Factor
k	Thermal Conductivity [W/Mk]
k_{cu}	Thermal conductivity of the copper [W/Mk]
L	Test Section Length [m]
$\dot{m}$	Mass flow Rate [kg/s]
Nu(x)	Local Nusselt Number
Nu_{avg}	Average Nusselt Number
P	Perimeter of the tube [m]
Pr	Prandtl Number
$\dot{Q}_e$	Electric Energy Supply Rate [W]
$\dot{q}_{in}$	Heat flux [W/m^2]
$\dot{Q}_f$	Heat Transfer Rate [W]
Ra	Raleigh Number
Re	Reynold Number
Ri	Richardson Number
Re_{cr}	Critical Reynold number
T_a	Ambient Temperature [°C]
T_i	Inlet Temperature [°C]
$T_f(x)$	Local Mean Fluid Temperature [°C]
$T_{si}(x)$	Inside wall temperature [°C]
$T_{so}(x)$	Outside wall temperature [°C]
V	Voltage [V]
x	distance from the tube inlet [m]

Greek Letters

ρ_{hnf}	density of the Hybrid nanofluids [kg/m^3]
ρ_{bf}	Base fluid density [kg/m^3]
ρ_p	Density of Particles [kg/m^3]
μ	Viscosity [kg/m. s]
ν	Kinematic viscosity [m^2/s]
ρ	Density [kg/m^3]
φ	Volume concentration

Subscripts

b	Bulk
w	Wall
p	Particles
O	Outlet/Out
i	Inlet
f	Fluid
s	Surface
a	Ambient/ Atmospheric
avg	Average
cr	Critical
hnf	Hybrid nanofluids
bf	Base fluid.
P	Particles
β	Coefficient of Thermal expansion
Φ	Free convection effects
Ω	Heat transfer Parameter (another form of Nusselt number)

Abbreviations

PWC	Percentage weight compositions
HTC	Heat Transfer coefficient
HNF	Hybrid Nanofluid
UWT	Uniform wall temperature
UHF	Uniform Heat flux"

transfer coefficients and affects the critical Reynolds number. Findings from Yasuo et al. [4] show that mixed convection (i.e., Buoyancy effects) affects the critical Reynolds number. Yasuo et al. [4] explained that if there are no disturbances, the critical Reynolds number decreases with a rise in the Rayleigh number value. This was believed to be due to the secondary flow (i.e., Buoyancy), which induced the turbulence and, as such, resulted in the flow transitioning to turbulence.

The presence of buoyancy-induced secondary flow typically causes free convection in tubes. The existence of these phenomena with forced convection heat transfer is termed mixed convection [5]. The effects of free convection on heat transmission behaviour often depend on the buoyant force's directions and the main flow [5]. The direction of the buoyant force in tube flow is critical to mixed convection heat transfer. Oliver et al. [6] explained that mixed convection can only improve the tube's heat transfer if the direction of the buoyant forces is the same as the main flow direction. Otherwise, the heat transfer coefficients would deteriorate. Li and Feng [7] revealed that mixed convection effects can be so significant that they can be comparable to forced convection, especially in situations where the flow rate is very low and there is a large heat flux. Oliver et al. [6] and Bergles et al. [8] explained that mixed convection effects in horizontal tubes can improve the heat transfer by about three to four times higher than values predicted by any theoretical forced convection correlations. Shome et al [9] state that the effects of the mixed convection phenomenon in the horizontal tube include increasing the fluid pressure drops. This was attributed to the creation of vortices by the excited fluid vapour. Secondary effects may also cause thermal stratification in the tube. Apart from the possible enhancement of heat transfer, the free convection effect can cause an early laminar flow transition to turbulence.

Early experimental research findings from nanofluids mixed convection heat transfer behaviour produced results contrary to the most numerically analysed data. The deterioration of the mixed convection behaviour of nanofluids has been discussed in a few relevant literatures. At the same time, an enhancement in the mixed convection heat transfer was noticed with the increase in volume concentration in the experimental work of Mansour et al. [10]. However, these findings were noticed to be inconsistent with the numerical work of Akbari et al. [11]. The work of Akbari et al. [11] shows that volume concentration was insignificant in the mixed convection heat transfer of the nanofluid. It's worth noting that both works of Akbari et al. [11] and Mansour et al. [10] used an inclined tube. But despite that, they produce different and incoherent findings. Tube inclination was also believed to have a peculiar and distinctive influence on mixed convection. Because, according to Derakhshan et al.[12]. The effects of the dispersed particles on mixed convection diminished with an increase in inclination angle. But the experimental work of Putra et al. [13], Wen et al. [14], Mansour et al. (Ben Mansour et al., 2011), and Li et al. [7] all reported that volume concentration decreases the mixed convection influence on the heat transfer.

Research on the mixed convection aspects of hybrid nanofluids has not been thoroughly investigated, especially with hybrid nanofluids. A literature survey shows that the numerical and experimental investigations only considered single nanofluids (i.e., nanofluids containing only one type of nanoparticles). Even with the single nanofluids, there are some significant discrepancies between the reported results, as cited earlier. The general hybrid nanofluid force convective heat transfer characteristics are still far from being fully understood. There are still some vital points that are not fully addressed. One of these areas is the transition region boundary condition. Research has shown that transition region boundary conditions depend on several important factors. Among these factors are inlet geometry, tube configurations, tube surface conditions, heat flux, mixed convection, etc. [15–19]. These were not the only ones; we just cited the most common ones. It's worth noting that most of the factors we have listed are related to one common aspect, which researchers believe to have been the main cause affecting the starting and ending of the transition flow regimes. This aspect is the flow disturbances. Nagendra et al. [20] believed that the transition from laminar to turbulent flow is mainly due to flow disturbances. The larger the disturbances, the greater the chances of the transition occurring. This was also the opinion shared by Ghajar et al. [15], Evert et al. [21] and Obot et al. [19]. They all explained that with the increase in fluid flow disturbances, the transition occurs much earlier than when the flow disturbances were low. Research work of Zontul et al. [22] and Tokgoz et al. [23] also indicates that tube geometry has a significant effect on the convective heat transfer characteristics. The interesting question here is the effects of the dispersed nanoparticles on the transition boundary. It's obvious that the presence of dispersed particles in the base fluid altered the fluid's thermal characteristics and its convective heat transfer behaviour. Another vital research question that needs to be considered is the effects of increased or decreased nanofluid volume concentrations on the transition boundaries. This question has also not been investigated with nanofluids. Ibrahim et al. [24] investigated the effects of particle size combination in the hybrid nanofluid mixture, and the results show that the transition boundary condition was significantly affected by the particle sizes. However, this research only considered one volume concentration (i.e., 0.3 vol) and the research focus was mainly on the particle's sizes. In a similar work, Ibrahim et al. [25] also reported that when the weight concentration of particles in the hybrid nanofluid varied, it affected the transition boundary. Therefore, in this research, we intend to investigate the influence of volume concentrations on the boundary conditions of hybrid nanofluids.

The entrance effect is another aspect of a hybrid nanofluid's forced convection heat transfer that has not been investigated thoroughly. This aspect was often neglected by the majority of researchers. Therefore, in most cases, this resulted in large discrepancies in experimental results from different researchers. Sometimes, entrance effects are mistaken for forced convection [25]. Because of the peculiar nature of nanofluids (e.g., high viscosity and presence of nanoparticle motions within the fluids), these effects tend to be more significant than they were with the base fluid. As such, neglecting or assuming their influence is negligible would be wrong. Under thermally developing flow, at the entrance regions, the thermal boundary layer is believed to be very thin [26]. Therefore, entrance effects can be noticed in the local Nusselt number. Because of the entrance effects on the local Nusselt number, we believe it's important to investigate its characteristics with regard to nanofluids. It's important to note that another critical issue that forces researchers to neglect the entrance effects or assume their effects are negligible is that it's very difficult to differentiate the entrance influence from mixed convection. Therefore, this aspect was often considered mixed convection in most cases [26]. Therefore, this research investigates the mixed conventions and entrance effects. We also investigate the best possible way to differentiate these two important phenomena.

Research by Shome et al [9] stresses that fluid properties like viscosity are often critical to its characteristics, especially with mixed convection. He specifically suggested that neglecting the effects of fluid viscosity on the fluid heat transfer is wrong. Especially when the temperature difference is significant, this effect of viscosity is important with nanofluids. Research findings show that viscosity increases with nanofluid volume concentration [27–29]. Therefore, it's paramount to investigate and quantify how this increase in viscosity due to volume concentration affects the mixed convection, entrance effects, and fluid flow boundaries of the hybrid nanofluid. Therefore, in this research work, we aim to investigate, characterise, and analyse the effects or influence of volume concentrations on the nanofluid's mixed convection heat transfer behaviour. Also, the research investigates the thermal entrance effects and transition boundaries characteristics of the nanofluid. Hybrid nanofluids of alumina oxide and multi-walled carbon nanotubes (i.e., MWCNT) were used (i.e., with water as the base fluid). Three volume concentrations of 0.3 %, 0.2 % and 0.1 % were prepared using a two-step method of nanofluid preparation and the experiments were conducted in a horizontal copper tube at a constant heat flux.

1.1. Hybrid nanofluid preparation

To investigate the effects of volume concentration on the heat transfer characteristics of this hybrid nanofluid (i.e., Al_2O_3 – MWCNT / water). Three-volume concentrations were prepared (i.e., 0.3 %, 0.2 %, and 0.1 % volume concentrations), using a two-step method. To prepare these fluids, nanoparticles, which are in powder form, were weighed and then dispersed into the base fluid (DI Water). To improve the fluid stability, a surfactant was added to the mixture, and the Surfactant used in this experiment was Sodium Dodecylbenzene Sulfonate (SDBS). To eliminate the nanoparticle agglomerations and have them properly disperse in the base fluid. Magnetic stirring and sonication processes were used. The mixture of dispersed nanoparticles and base fluids was subjected to 30 min of magnetic stirring, followed by a sonication process for about 90 min. This procedure was adopted from Anoop et al. [30], Nadooshan et al [31] and Ibrahim et al. [24]. Fig. 1a and 1b below show the hybrid nanofluid's SEM (i.e., Fig. 1a) and TEM images (i.e., Fig. 1b).

Hybrid nanofluid Stability was examined by measuring and monitoring its viscosity at a constant temperature of 25 °C. The viscosity readings were taken using the SV–10 Vibro Viscometer (A&D, Japan), which is set to record and log data in at an interval of 10 min for about 6 hr 30 min, as shown in Fig. 1c**.** The results indicate that the prepared nanofluid (Al_2O_3 – MWCNT / water) has shown good and satisfactory stability during the period. The time duration of 6 h, 30 min was chosen because it takes roughly between 3 and 3.5 h to complete the experiments. This indicates that the fluid would maintain a very good and satisfactory stability throughout the experiments. A similar method was also used by Osman et al.[32] and Giwa et al. [33,34] and Ibrahim et al. [35]. Fluids were also visualised for 10 days without any visible sedimentation, which reaffirmed their good stability.

Eqs. (1) and (2) were applied to determine the heat capacity and density of the hybrid particles [35,36].

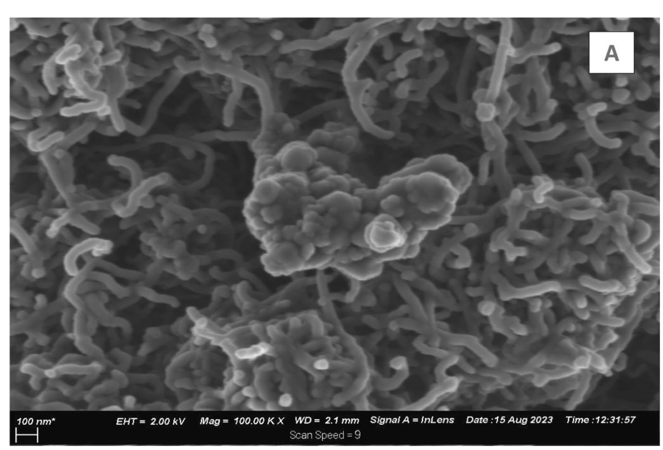

Fig. 1a. SEM image of the Hybrid Nanofluid.

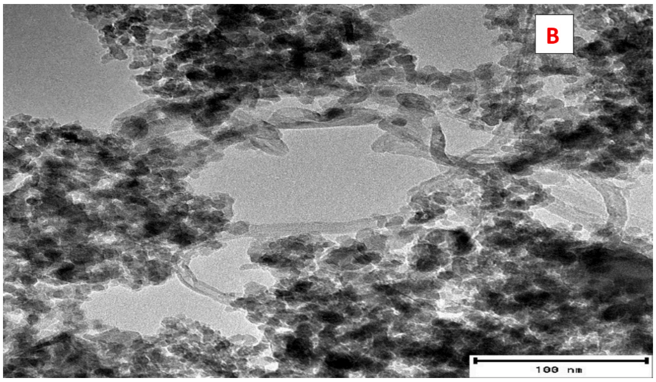

Fig. 1b. TEM image of the nanofluid.

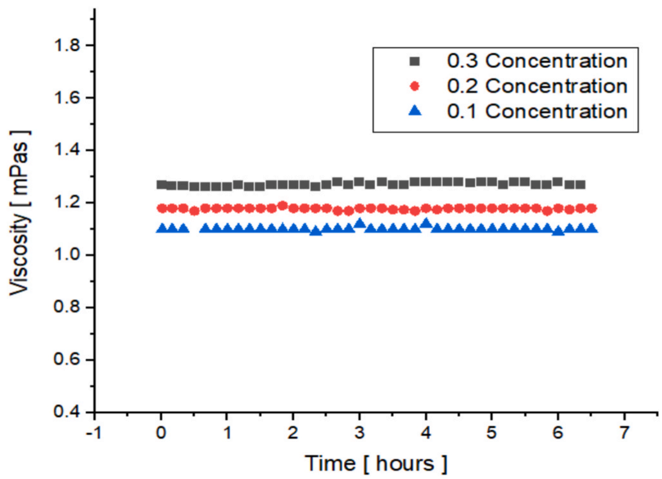

Fig. 1c. Al_2O_3 – MWCNT / water Nanofluids Stability Test at 25 °C for 6 hr 30 min.

$$\rho_{(Al_2O_3-MWCNT)} = \frac{(\rho_{Al_2O_3}PWC_{Al_2O_3}) + (\rho_{MWCNT}PWC_{MWCNT})}{(PWC_{Al_2O_3} + PWC_{MWCNT})} \quad (1)$$

$$C_{(Al_2O_3-MWCNT)} = \frac{(C_{Al_2O_3}PWC_{Al_2O_3}) + (C_{MWCNT}PWC_{MWCNT})}{(PWC_{Al_2O_3} + PWC_{MWCNT})} \quad (2)$$

Using mixture rules as given in Eqs. (3) and (4) by Naik et al. [37], the hybrid nanofluid's specific heat capacity and density (i.e., Al_2O_3 – MWCNT) were estimated.

$$\rho_{hnf} = (1-\varphi)\rho_{bf} + \varphi\rho_p \quad (3)$$

$$c_{hnf} = (1-\varphi)c_{bf} + \varphi c_p \quad (4)$$

1.2. Nanofluids thermal conductivity

The thermal conductivity of the prepared nanofluids was measured using a KD2 pro thermal conductivity meter. The measurements were taken between the temperatures of 10 °C and 30 °C.

Measurement was conducted within an error limit of less than 0.1 for all the volume concentrations prepared. Results show that (i.e., Fig. 2) the thermal conductivity decreases with the decrease in volume concentration.

1.3. Nanofluid viscosity

Hybrid nanofluid viscosity measurement was taken between 20 °C and 50 °C temperatures. Sv–10 Vibro Viscometer, manufactured by

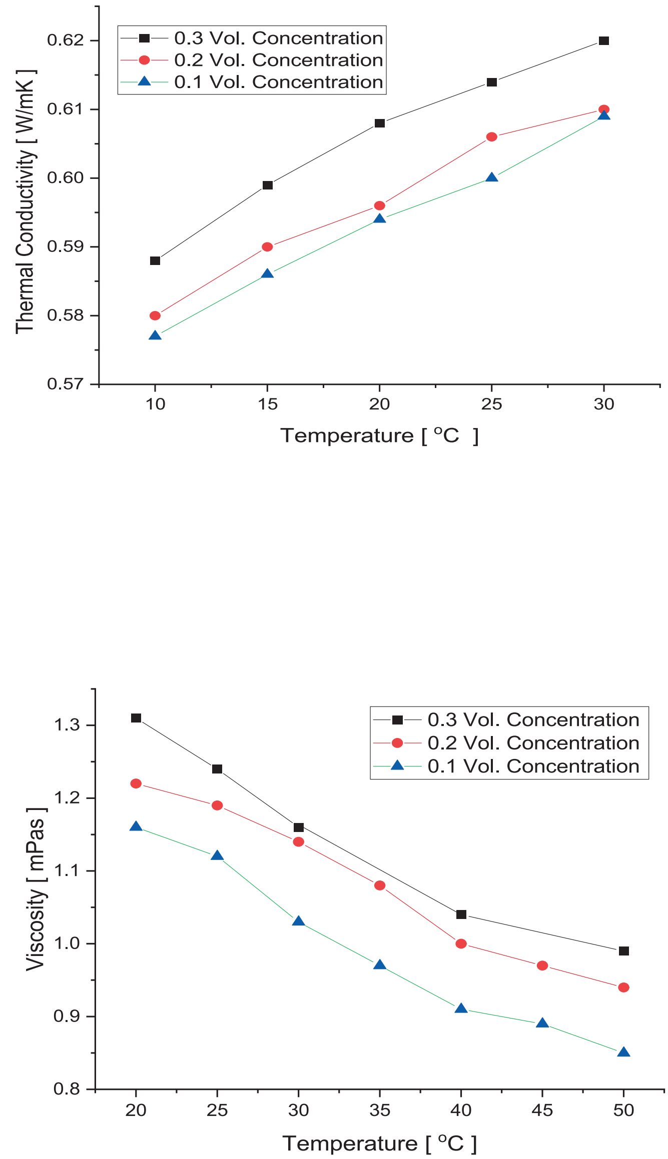

Fig. 2. Thermal Conductivity and Viscosity of the Hybrid Nanofluids.

A&D, Japan, was used. At its full capacity, this instrument has an average uncertainty value of less than 0.05 (i.e., 5 %). Results indicate that hybrid nanofluid viscosity depends on both temperature and volume concentration. 0.3 vol concentration has the highest viscosity, followed by 0.2 and 0.1. Research has already shown that hybrid nanofluid viscosity decreases with the increase in temperature [38], which corresponds to our research findings in Fig. 2.

1.4. Experimental setup

This research was conducted with the same experimental set used in Ibrahim et al. [24] and Ibrahim et al. [25]. But for clarity, a brief description of the key component of the setup will be given here.

The setup was equipped with high-precision equipment like a Coriolis flow meter (4) (i.e., CmFs015) with an operation capacity between 0.204 kg/min to 4.09 kg/min which has an accuracy of about 0.05 % at full operation state, gear pump (1), Thermal bath (*Thermostatic water bath)* (6), power supply (i.e., KIKUSUI PWR800M) and Data acquisition system DAQ. The system also has a storage tank with a capacity of 10 L for storing nanofluids during the experiment. The diagram of the experimental setup is presented in Fig. 3. The test section was made from

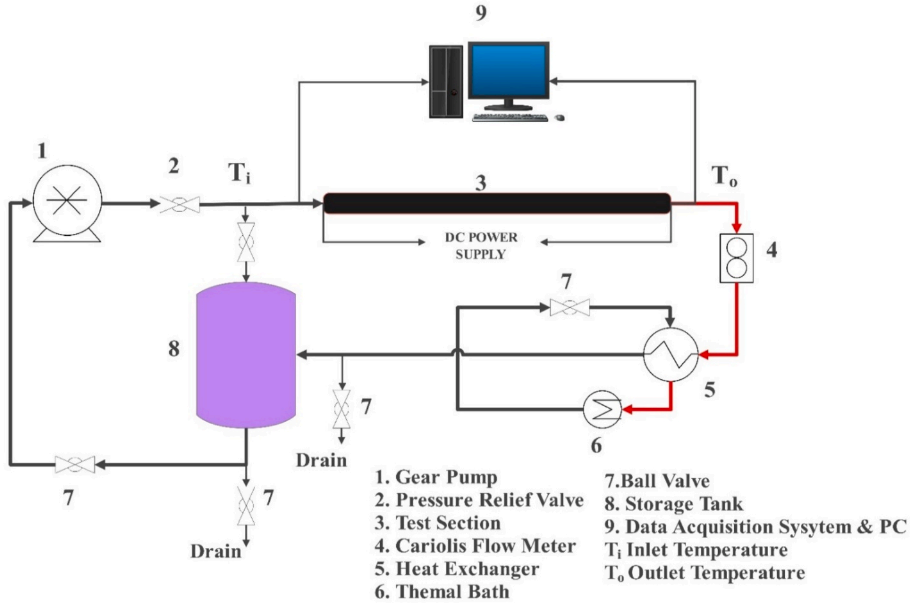

Fig. 3. Schematic Diagram representing the experimental setup layout.

copper materials. The test section was connected to the power supply, which supplied a constant heat flux that heated the fluid to a temperature. T_i (i.e., inlet temperature) to T_e (i.e., output temperature). The fluid exited the test section via the flow meter (4). The hot fluid, or nanofluid, heated from the test sections (3), was cooled using a tube-in-tube heat exchanger (5). Water from a thermal bath (6) was made to circulate through the tube-in-tube heat exchanger (5), and the heat from the nanofluids was absorbed, maintaining a steady temperature at the inlet. The system had a data-capturing device that processed the signals and information it received from the power supply, flowmeters, thermocouples, and other sources with the aid of a desktop computer (9). The computer uses a LabVIEW program that was set up to log data at 20 Hz.

1.5. Test section

The schematic design of the test section used in this experiment is given in Fig. 4. The test section has two mixers positioned at the inlet and outlet of the heat exchanger. The heat exchanger section of the test section has a total length of 1000 mm, while the hydrodynamic entrance length of the test section is 500 mm. The hydrodynamic length of the test section was calculated using the correlation of Dust et al. [39] given in Eq. (5).

$$\frac{L}{D} = \left[(0.619)^{1.6} + (0.0567\mathrm{Re})^{1.6}\right]^{\frac{1}{1.6}} \tag{5}$$

A copper tube with external and internal diameters of 9.5 mm and 8 mm was used to construct the test sections (i.e., both the hydrodynamic length and heat exchanger). A total of about 28 T-type thermocouples were used on the heat exchanger. These thermocouples were positioned at seven measuring positions on the test section wall. (i.e., each position with a total of four thermocouples). The seven thermocouple positions are 120 mm, 250 mm, 380 mm, 510 mm, 640 mm, 770 mm, and 900 mm from the test section inlet. Also, a thermocouple was placed at the test section inlet and outlets, which measured the fluid inlet and outlet temperatures (i.e., T_i and T_o). The heat exchanger part of the test section was insulated with six layers of insulation material. This helps minimise heat loss in the surroundings. This helps to minimise heat loss to the barest minimum. The calculated heat lost to the surroundings is maintained at about 4 %. For heating the heat exchanger, a Constantine wire was used. A total of 8.67 kW/m^2 heat flux was supplied to the heat exchanger during the experiments.

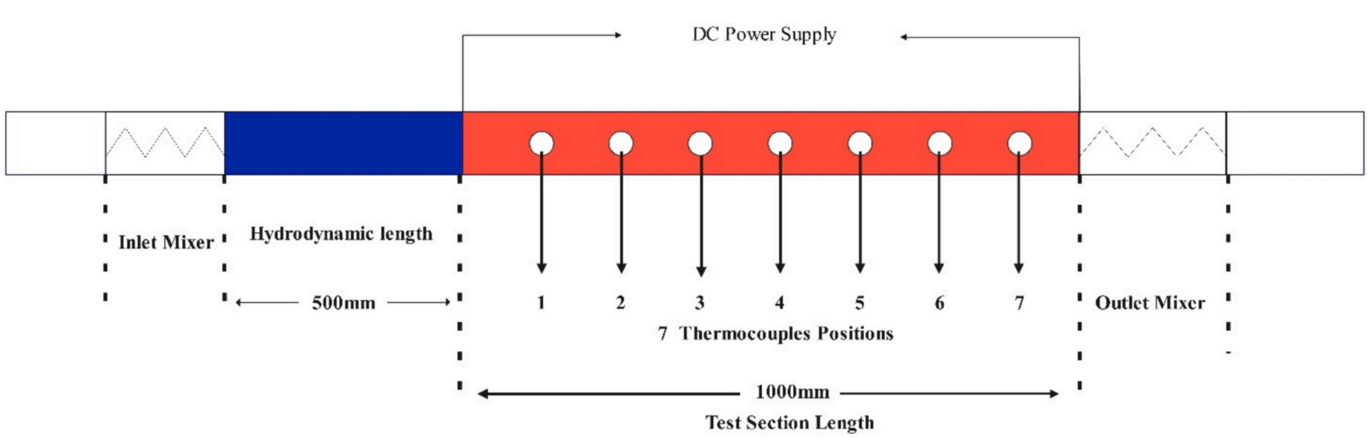

Fig. 4. Schematic Diagram of the Test Section.

1.6. Experimental procedure

To reach a steady state condition, the system must be allowed to operate for at least ninety minutes (i.e., 90 min). A steady state is said to have been achieved when there are no discernible temperature, pressure, or flow rate changes. When the system was stabilised, a new flow rate for data capturing was obtained by making very small adjustments to the flow rates. After altering the flow rate, the system takes around ten minutes to stabilise and capture new readings. Readings were taken from the higher to the lower flow rate. This was done to reduce the amount of leftover heat that might be stored in the insulation, which may affect the subsequent readings to be taken. 200 measurement readings were taken for every data point by the DAQ system and averaged for analysis.

1.7. Data analysis

Data analysis used in this research was adopted from the work of Meyer et al. [40] and Ibrahim et al. [25].

1.8. Heat transfer

The nanofluid coefficient of heat transfer $h(x)$ was computed from the relation given in Eq. (6).

$$h(x) = \frac{\dot{q}_{in}}{T_{si}(x) - T_f(x)} \tag{6}$$

$\dot{q}_{in}$ is the supplied heat flux to the system, calculated from the heat transfer rate $\dot{Q}_f$.

$$\dot{q}_{in} = \frac{\dot{Q}_f}{A_s} \tag{7}$$

The heat transfer rate $\dot{Q}_f$ to the nanofluid were determined using mass flow rate, inlet temperature, outlet temperatures and specific heat capacity of the hybrid nanofluids at bulk temperature. The relation was given in Eq. (8).

$$\dot{Q}_f = \dot{m}c_p(T_{out} - T_{in}) \tag{8}$$

A_s is the internal tube surface area, and its expression was given in Eq. (9).

$$A_s = \pi DL \tag{9}$$

1.9. Energy supplied

$$\dot{Q}_e = VI \tag{10}$$

Internal tube surface temperature $T_{si}(x)$ and $T_f(x)$ nanofluid's (i.e., local fluid's temperature) were computed using outer wall temperature $T_{so}(x)$ measured at bulk fluid temperature (i.e., Eqs. (11) and (13). (R_w) is the resistance through the tube wall, and its expression is given in Eq. (12).

$$T_{si}(x) = T_{so}(x) - \dot{q}_{in}R_w \tag{11}$$

$$R_w = \frac{\ln\frac{D_{so}}{D_{si}}}{2\pi k_{cu}L} \tag{12}$$

$$T_f(x) = T_i + \frac{\dot{q}_{in}xp}{\dot{m}c_p} \tag{13}$$

Where:

k_{cu} The thermal conductivity of the tube material (i.e., copper) is defined by [41] and applied by Meyer et al. [28], While p it is the perimeter.

Nanofluid's average heat transfer coefficient h_{avg} was computed using the average local heat transfer coefficient $h(x)$ (i.e., Eq. (6).

$$h_{avg} = \frac{(h(x_1) + h(x_2) + h(x_3) + \ldots\ldots..h(x_n))}{n} \tag{14}$$

Where n = 7, which signifies the number of measurement positions on the heat exchanger.

Nanofluid's Reynolds number and Prandtl number were obtained from the relations in Eqs. (15) and (16).

Reynolds Number (i.e., *Re)*

$$\mathrm{Re} = \frac{4\dot{m}}{\pi DL} \tag{15}$$

Prandtl Number (i.e., *Pr)*.

$$Pr = \frac{\mu c_p}{k} \tag{16}$$

Average Nusselt (i.e., Eq. (17) was computed from the average convective heat transfer coefficient (h_{avg} relation given in Eq. (14)).

$$Nu_{avg} = \frac{h_{avg}D}{k} \tag{17}$$

k It is the thermal conductivity of the fluids. For the base fluid (i.e., DI water), the thermal conductivity was calculated using the Popiel et al. [42] correlations at bulk temperature, i.e.. While the thermal conductivity of the nanofluids was estimated at bulk fluid temperature T_b using the Pak and Cho [43] correlations in Eq. (18). Meanwhile, for viscosity, a similar procedure was followed by Sharma et al. [38], Osman et al. [39], and Ibrahim et al. [31]. That is, using a regression Eq. (19).

$$k_{nf} = k_w(1 + 7.47\varphi) \tag{18}$$

$$\mu_{nf} = \mu_w(1 + 2.5\varphi + 6.2\varphi^2) \tag{19}$$

Colburn J factors

$$j = \frac{Nu}{\mathrm{Re}Pr^{1/3}} \tag{20}$$

1.10. Mixed convection analysis

The method used to evaluate the mixed convection heat transfer analysis was adopted from Feng et al. [44] and Ibrahim et al. [25] This method used Eqs. (21) and (22) to calculate the nanofluids Graetz Number and Grashof Number, respectively. Raleigh Number (Ra) and Richardson Number (Ri) were obtained from Eqs. (23) and (24), respectively.

$$Gz = \frac{\pi}{4}\mathrm{Re}Pr\frac{D}{L} \tag{21}$$

$$Gr = \frac{g\beta(T_s - T_m)D^3}{\upsilon^2} \tag{22}$$

$$Ra = GrPr \tag{23}$$

$$Ri = \frac{Gr}{\mathrm{Re}^2} \tag{24}$$

The hybrid nanofluid natural convection influence was analysed using the procedure followed by Feng et al. [44]. In this method, Feng et al. [44] expressed that based on the supplied heat flux to the heat exchanger (i.e., Uniform wall temperature condition (UWT) or Uniform Heat flux conditions (UHF)). A simplified average Nusselt number of relations can be expressed as given in Eq. (25).

$$Nu_F\left(\frac{\mu_w}{\mu_b}\right)^{0.14} = \begin{cases} 1.75Gz^{1/3}\ldots\ldots\ldots\ldots\ldots\ldots\ldots\ldots(UWT) \\ 2.11Gz^{1/3}\ldots\ldots\ldots\ldots\ldots\ldots\ldots\ldots(UHF) \end{cases} \tag{25}$$

While the expression of G_z It can be summarised as given in Eq. (26).

$$Gz \geq 26.2\left(\mathrm{Re}Pr\frac{D}{L} \geq 33.3\right) \tag{26}$$

As suggested by Shome et al. [9], the influence of viscosity is very significant on mixed convection, especially when the temperature difference is significant. Therefore, it has to be considered. Therefore $\left(\frac{\mu_w}{\mu_b}\right)^{0.14}$ was added, which accommodates the radial variation of viscosity. [6,45,46]. The generalised equation is given in Eq. (27).

$$Nu\left(\frac{\mu_w}{\mu_b}\right)^{0.14} = A(Gz + \Phi)^{1/3} \tag{27}$$

From Eq. (27), ϕ can be expressed in terms of the Grashof, Prandtl and Graetz numbers. This was given in Eq. (28).

$$\Phi = \left[\frac{1}{2.11}Nu\left(\frac{\mu_w}{\mu_b}\right)^{0.14}\right]^3 - Gz \tag{28}$$

According to Feng et al. [44], parameter ϕ, or ϕ /Gz, signifies the impact of the free convection. The higher the ϕ or ϕ /Gz, the greater the significance of natural convection.

However, Yang et al. [29] explained that, when analysing mixed convection influences on the Reynolds and Nusselt numbers, using a parameter, 'Ω, would be more appropriate. The mathematical expression of 'Ω was given in Eq. (29) [29,44].

$$\Omega = Nu\left(\frac{\mu_w}{\mu_b}\right)^{0.14}\left(Pr\frac{D}{L}\right)^{-1/3} \tag{29}$$

Using Eqs. (21) and (29), Eq. (25) was rewritten and given in Eq. (30). Yang et al. [29].

$$\Omega_F = Nu\left(\frac{\mu_w}{\mu_b}\right)^{0.14}\left(Pr\frac{D}{L}\right)^{-1/3} = 2.11\left(\mathrm{Re}\frac{\pi}{4}\right)^{1/3} = 1.95\mathrm{Re}^{1/3} \tag{30}$$

Therefore, in this research, Eq. (30) will serve as the benchmark by which we assess the strength of the mixed convection. This was in accordance with Yang et al. [29], Ibrahim et al. [25] and Feng et al. [44]. The higher the deviations of the research data from Eq. (30), the higher the influence of the natural convection [29].

Eqs. (23), (24) and (28) also assessed the volume concentration effects on the mixed convection, especially at the transition region.

1.11. Validations of the experimental setup

This setup was validated under both forced and mixed convection conditions. Ibrahim et al. [22] and Ibrahim et al. [23] gave a detailed analysis of the validation process. But for clarity, a brief description of the results is given here.

The setup was validated according to the procedure analysis used by Feng et al. [44] and Osman et al. A base fluid was used to validate the system. This experiment validated the setup within the Reynolds number range of 1000 and 6000. This range covers the Reynolds number range that is of interest in this research. Verified correlations from the Cengel and Ghajar [47] and Osman et al. [32]. Along the turbulent region, correlations of Notter and Rouse, and Dittus–Boelter [47] were used. They validated the experimental data from the setup within an average deviation of about 8 %, as shown in Fig. 5a. The correlation between Morcos and Bergles and Depew and August was used to validate the data in the laminar region. Depew and August's correlations validated the result with a maximum deviation of about 10 % Fig. 5b. while the correlation of Morcos and Bergles validates the result within a maximum deviation of 11 %. These two correlations (i.e., Morcos and Bergles, and Depew and August correlations) were specifically developed for laminar mixed convection conditions. These results show that the setting and setup function reasonably well.

(1) Dittus – Boelter Correlation

$$Nu = 0.023\mathrm{Re}^{0.8}Pr^{0.4} \tag{31}$$

(2) Correlation of Depew and August

$$Nu = A\left(\frac{\mu_b}{\mu_w}\right)^{0.14}\left[Gz + C\left(GzGr^{1/3}Pr^{0.36}\right)^{0.88}\right]^{1/3} \tag{32}$$

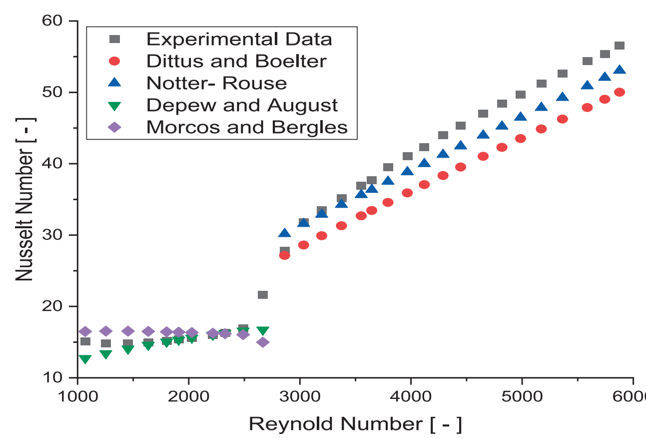

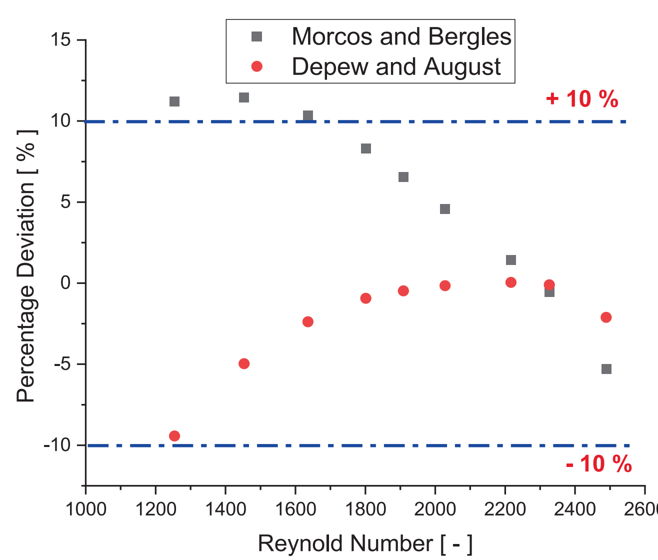

Fig. 5. A) experimental Nusselt data for DI-water (i.e., base fluid) compared to the standard correlations. b) Percentage deviation of the laminar experimental water data (i.e., base fluid) with mixed convection correlations.

Parameter A has a value of 1.75 or 2.11, depending on the heat flux conditions. In contrast, parameter C has a constant value of 0.12.

(3) Morcos and Bergles' correlations

$$Nu = \sqrt{\left[(4.36)^2 + \left[0.145\left(\frac{Gr^*Pr}{pw_f^{0.25}}\right)^{0.265}\right]^2\right]} \tag{33}$$

Were.

$Gr^* = GrNu$ is the modified Grashof Number,

Pw_f is given as.

$$pw_f = \frac{hd}{k_w t}$$

(4) Notter and Rouse's relations

$$Nu = 0.015\mathrm{Re}^{0.856}Pr^{0.347} \tag{34}$$

1.12. Uncertainty analysis

Experimental uncertainties were estimated using a method adopted from the work of Osman et al. [32], Everts et al. [48], and Dunn et al. [49]. This method used Eqs. (35)–(40) to determine the experimental data uncertainties for the convective coefficient of heat transfer, Nusselt number, and Reynold number (Re). It was discovered that the average uncertainties for the Nusselt number, coefficient of heat transfer, and Reynolds number were approximately 4 %, 6 %, and 5 %, respectively. The average uncertainty of Gr was found to be approximately less than 6 %. While that of Ra, and Ri were found to be less than 5 %.

$$\delta Nu = \left[\left(\frac{\delta Nu}{\delta h}\delta h\right)^2 + \left(\frac{\delta Nu}{\delta D}\delta D\right)^2 + \left(\frac{\delta Nu}{\delta k}\delta k\right)^2\right]^{1/2} \tag{35}$$

$$\delta h = \left[\left(\frac{\delta h}{\delta \dot{q}}\delta \dot{q}\right)^2 + \left(\frac{\delta h}{\delta T_S}\delta T_S\right)^2 + \left(\frac{\delta h}{\delta T_b}\delta T_b\right)^2\right]^{1/2} \tag{36}$$

$$\delta \mathrm{Re} = \left[\left(\frac{\delta \mathrm{Re}}{\delta \dot{m}}\delta \dot{m}\right)^2 + \left(\frac{\delta \mathrm{Re}}{\delta D}\delta D\right)^2 + \left(\frac{\delta \mathrm{Re}}{\delta A_c}\delta A_c\right)^2\right]^{1/2} \tag{37}$$

$$\begin{aligned}\delta Gr = \Bigg[&\left(\frac{\delta Gr}{\delta \beta}\delta\beta\right)^2 + \left(\frac{\delta Gr}{\delta p}\delta p\right)^2 + \left(\frac{\delta Gr}{\delta Ts}\delta Ts\right)^2 + \left(\frac{\delta Gr}{\delta Tm}\delta Tm\right)^2 \\ &+ \left(\frac{\delta Gr}{\delta D}\delta D\right)^2 + \left(\frac{\delta Gr}{\delta \mu}\delta\mu\right)^2\Bigg]^{1/2}\end{aligned} \tag{38}$$

$$\delta \mathrm{Ra} = \left[\left(\frac{\delta \mathrm{Ra}}{\delta Gr}\delta Gr\right)^2 + \left(\frac{\delta \mathrm{Ra}}{\delta Pr}\delta Pr\right)^2\right]^{1/2} \tag{39}$$

$$\delta \mathrm{Ri} = \left[\left(\frac{\delta \mathrm{Ri}}{\delta Gr}\delta Gr\right)^2 + \left(\frac{\delta \mathrm{Ri}}{\delta \mathrm{Re}}\delta \mathrm{Re}\right)^2\right]^{1/2} \tag{40}$$

2. Results and discussion

2.1. Effects of volume concentration on the start and end of the transitions

Different methods were suggested or used in determining the critical Reynolds number. For example, Meyer and Bolarin [50] used a line method to identify the critical Reynolds on the Colburn-Reynolds graph, where a curve fit method is used to draw a line through the laminar and transition points. In this method, the point where these two lines intersect was regarded as the critical (Rcr), Reynolds number (i.e., the start of the transition regime). But Ghajar and Strickland [51] suggested another method for estimating the critical Reynolds number, as represented in Eq. (41). This method was also used by Everts and Meyer [26] and Andrade et al. [52]. In this current research work, both the two methods of Meyer and Bolarin [50] and Ghajar and Strickland were considered and discussed. In Fig. 6, the Everts and Meyer [26] method was presented. In this procedure, the Critical Reynolds number ($\mathrm{Re_{cr}}$) is defined as the Reynolds number where the gradient of the Colburn J factors with respect to the Reynolds number changes from negative to positive.

Mathematically, this was expressed in Eq. (41).

Re= Re_{cr}, When

$$\mathrm{Re} = \left(\frac{dj}{d\mathrm{Re}}\right) = 0 \tag{41}$$

The critical ($\mathrm{Re_{cr.}}$) The Reynolds number of the three-volume concentrations 0.3, 0.2, and 0.1 was identified using Eq. (41) and represented in Fig. 6. Results show that the transition started at different critical Reynolds ($\mathrm{Re_{cr}}$) numbers for the three fluids (i.e., 0.3, 0.2, and 0.1). Transition starts at an approximate critical Reynolds numbe$_{\mathrm{r.}}$ ≈ 2020 for 0.3 concentration, while 0.2 and 0.1 concentration at an approximate critical Reynolds of 2050 and 2300, respectively. Fig. 6b and c. The difference in the critical Reynolds number (Recr) of the fluids can be due to the different concentrations of the dispersed particles in the base fluid. This affected the fluid properties and increased the fluid disturbances, as explained by Nagendra et al. [20]. Compared to the base fluid, the transition occurred earlier with the nanofluid (i.e., 0.3 % volume concentration) than with water. Because with the base fluid transition has started at the Reynolds number of $\mathrm{Re_{cr.}} = 2540$ Fig. 6d. The transition was delayed the most with 0.1 % volume concentration ($\mathrm{Re_{cr.}} = 2300$) as compared to the other volume concentrations (i.e., 0.2 and 0.3 %). This shows that an increase in the particle concentration results in the earlier occurrence of the transition.

From Fig. 7. The line method was used to identify the start of the transitional flow for the three-volume concentration. One important reason for using this method is that it's much easier than Eq. (41) and gives an approximate value of the critical Reynolds. From Fig. 7a, Colburn J factor data for 0.3 vol concentration were plotted against the Reynolds number. Using the line method, results show that the critical Reynolds number of 0.3 % volume concentration is 2140 ($\mathrm{Re_{cr}} \approx 2140$). From Fig. 7b and c, the respective critical Reynolds numbers of 0.2 % and 0.1 % volume concentration were found to be $\mathrm{Re_{cr}} \approx 2200$ and $\mathrm{Re_{cr}} \approx 2330$, respectively.

When compared to the value of the critical Reynolds number identified using equation (41) and the line methodTable 1 shows that the values differ slightly, especially with the 0.3 % and 0.2 % volume concentrations. The critical Reynolds values using Eq. (41) differ by 5.6 % compared to the value obtained from the line method for 0.3 % concentration. And with a 0.2 % concentration, it only differs by 6.95 %. However, with 0.1 % volume concentration, the deviation from Eq. (41) was only 1.3 %.

The flow regime boundary has been a subject of discussion for quite a long time. Conventionally, laminar, transition, and turbulent boundaries were identified qualitatively or based on visual observation, making it very difficult to objectively produce consistent results on the flow boundaries [53]. However, these two methods have something in common: we can objectively categorise the flow regimes with a certain degree of accuracy.

2.2. Effects of volume concentration on the range of transition

The range of the transitions can easily be described as the Reynolds numbers or the length of the Reynolds numbers, which takes the flow before it becomes fully turbulent. To identify the range of the

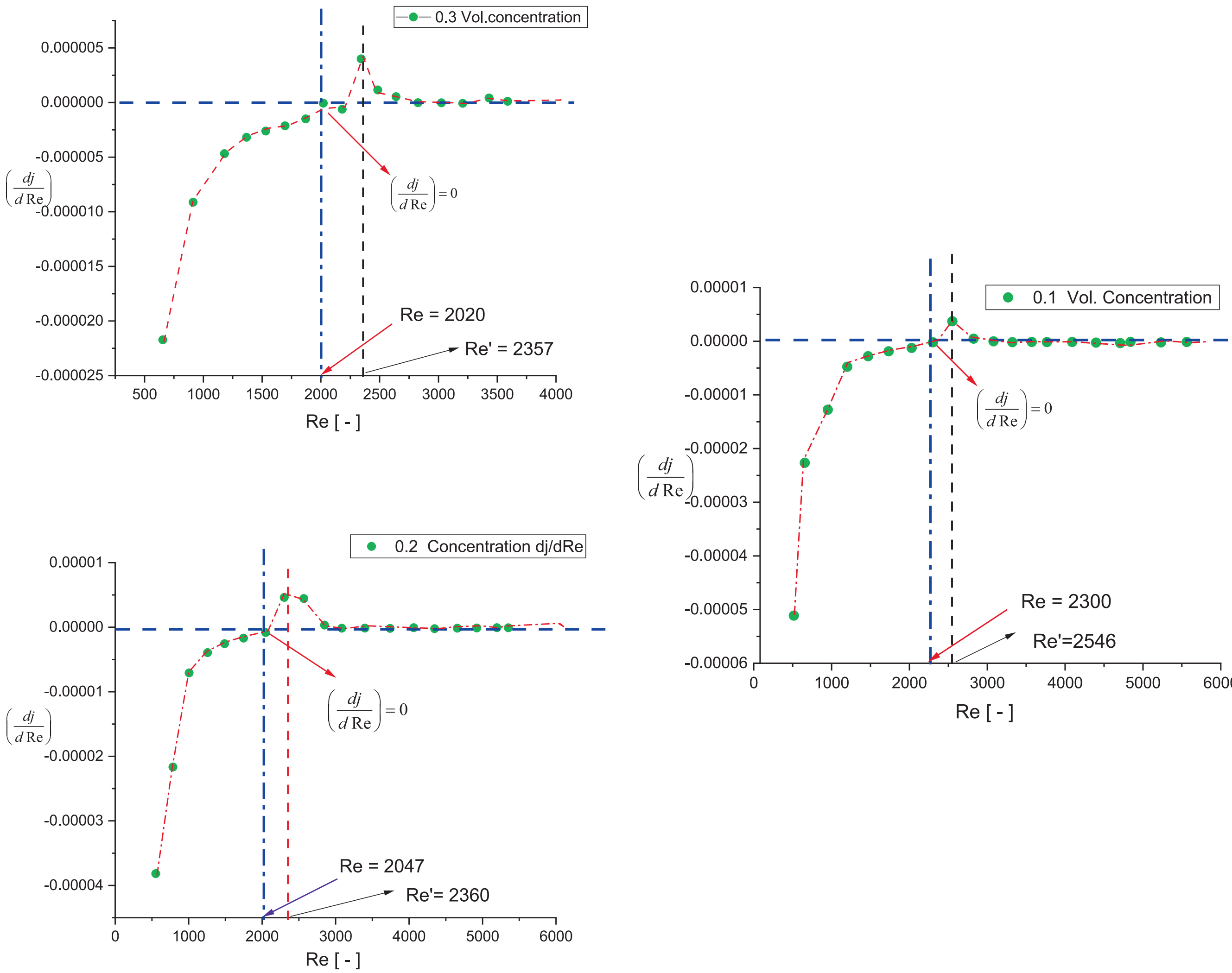

Fig. 6. Graph of Colburn J Factor gradient against Reynolds number.

transitions, we must first identify the end of the transitional flow. The end of the transition is the Reynolds number at which the flow becomes fully turbulent. This point was also subjected to a discussion from different research views. Some researchers are of the opinion that there is another flow regime after the transitional regime. Where the flow is not fully turbulent, and its characteristics differ significantly from those of the transition regime [26]. This region is considered as the quasi-turbulent flow regime [26]. The most significant feature of this flow regime is that the theoretical turbulent correlations largely failed to predict its Nusselt number value. Empirical correlations often over-predicted the Nusselt values at this flow region (i.e., Quasi-turbulent regime). However, this region is often considered a section or part of the transition regime in most research. Because there are no clear distinctions between the regime and the transition regime, for example, Meyer and Bolarin [50] could only distinguish the quasi-turbulent region from the transition region using the average frequency fluctuation. In the transition region, the average fluctuation frequency was 1/20 Hz, while in the quasi-turbulent region it was 1/10 Hz.

However, one crucial factor that was raised regarding this region (i.e., quasi-turbulent) was that the regime properties are not very different from those of the transition region. But Everts and Meyer et al. (Everts & Meyer, 2018) insisted that the flow characteristics along the quasi-turbulent regime are very similar to the turbulent regime rather than the transition regime. Their findings show a slight difference between their temperature standard deviation (Everts & Meyer, 2018). Similar findings were reported by Meyer et al. [50]. However, in most of the research works that involved highly viscous fluids like ethylene glycol and molten salt, this regime was hardly noticed [7,44,54]. Everts et al. [26] said it is very hard to identify the start and ending points of the quasi-turbulent region [26]. This can be seen clearly from Meyer and Bolarin [50], where the regime was not considered as a separate region. But it was rather included in the transition region. This was also in accordance with Abraham et al. [55], Yasuo et al. [4], Andrade et al. [52] and Sieder et al. [56], who all included this region as part of the transition region.

In this research, the results of the line method will be adopted to categorise and classify this hybrid nanofluid flow boundary. Using the line method, the end of the transition regime will be regarded as the point at which the turbulent flow fully starts. Meyer and Bolarin [50] describe this point as the point where the line of best fit from the turbulent regime (line T–T) intersects with the line of best fit from the transition region (i.e., line L–L). The end of the transition regime of the three different concentrations of this hybrid nanofluid is identified in Fig. 7. Results show that the transition with 0.3 % volume concentration ended much earlier than the other volume concentrations (i.e., 0.2 and 0.1). The transition appeared to have ended at a Reynolds number of 2580, with 0.3 % concentration.

Meanwhile, for other concentrations (i.e., 0.2 % and 0.1 %), the transition end was found to be around the Reynolds number of 2700 and 2750, respectively. Several factors may be responsible for these

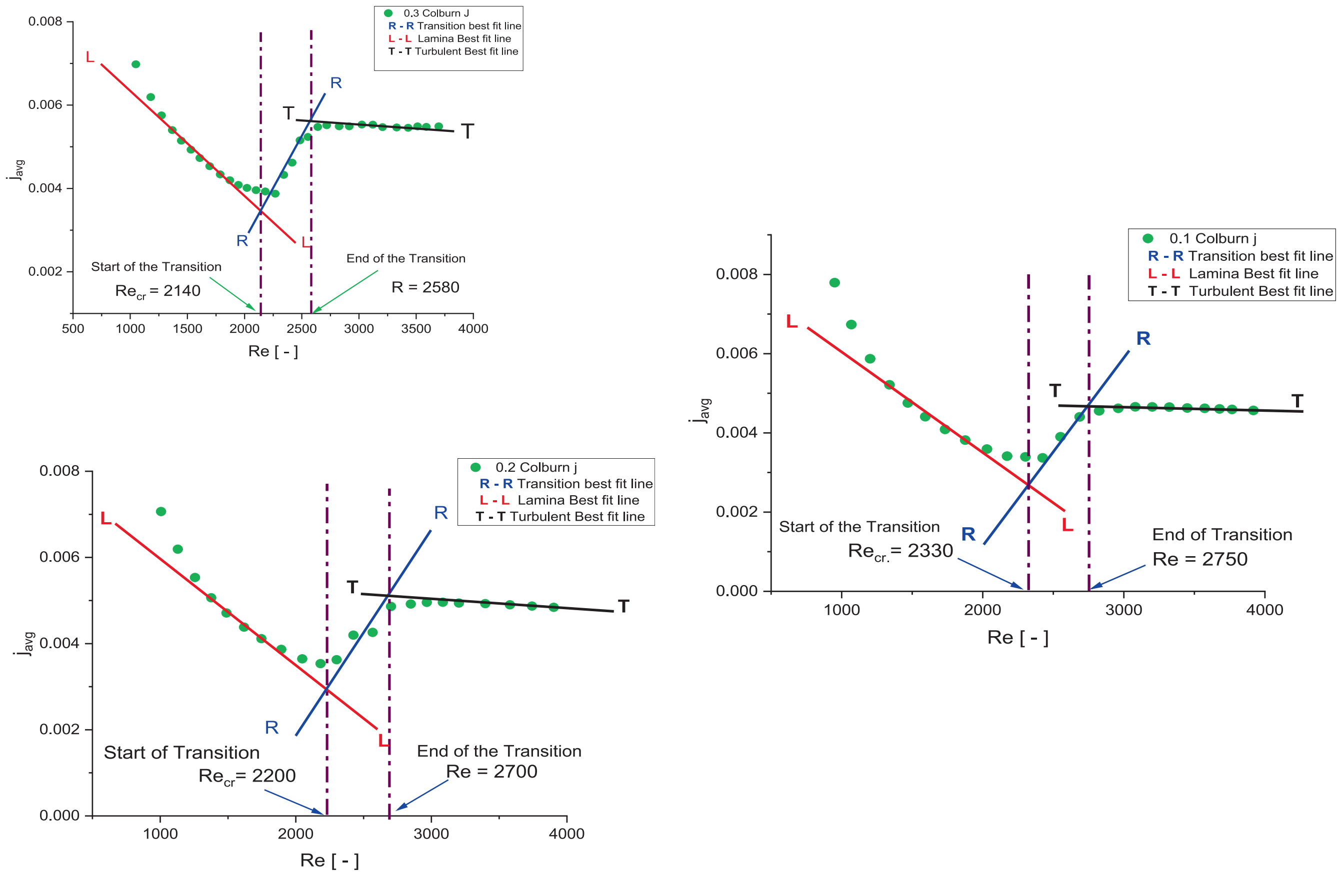

Fig. 7. Identifying Critical Reynolds Number Using the Line Method.

Table 1
Comparison of the start of the transition regime from the two methods.

		Vol. Con.	Line Method	Eq. (41)
S/N	Fluid	Vol. conc.	Start of the Transition	Start of the Transition
1	Hybrid Nanofluid	0.3	2140	2020
2	Al2O3 and	0.2	2200	2047
3	MWCNT	0.1	2330	2300

differences. The most obvious are viscosity and mixed convection. Yasuo et al. [4] found that mixed convection or the presence of the secondary flow may also affect the start and end of the transition flow regime. Dispersing nanoparticles in the base fluid proves to have altered the base fluid's heat transfer characteristics in every aspect. These variations of the transition endpoint can be largely attributed to the increase in viscosity due to volume concentration and temperature gradient.Table 2

Table 3 provides the boundary ranges for the three-volume concentration considered in this research. These ranges were determined using the line method (i.e., Critical Reynolds number of the flow) from Fig. 7. It is also important to note that the data in Fig. 7 are based on the

Table 2
Range of transition regime using line method.

			Line Method	
S/N	Fluid	Vol. conc.	Start of the Transition	End of the Transition
1		0.3	2140	2580
2		0.2	2200	2700
3		0.1	2330	2750

Table 3
Range of laminar regime for the three-volume concentration.

S/N	Volume Concentration	Laminar Range	Critical Reynolds Number
1	0.3	1000 to 2140	2140
2	0.2	1000 to 2200	2200
3	0.1	1000 to 2330	2330

average Colburn J (i.e., J_{ave}). Therefore, the effects of axial positions are not considered.

2.3. *Influence of axial position*

Fig. 8 shows the effects of the tube axial position on both the laminar, transition and turbulent regimes. Many conditions are believed to have made the axial tube position very influential on the heat transfer. One of which is the temperature gradient along the tube. The temperature gradient is essential, especially regarding nanofluids, because of their high viscosity, thermal conductivity, and specific heat capacity. This resulted in the variation in heat transfer properties along the tube. From Fig. 8 it can be seen that the transition appeared to have started at slightly different critical Reynold for a particular tube position, for example at an axial distance of $x/d = 15$, the transition critical Reynold number is 2209, while at $X/D = 112.5$, the critical Reynold number is 2250, as we explained earlier this was basically due to the influence of the temperature gradient and thermal entrance effects.

Ghajar and Tam [53] explained that the increase in temperature gradient along the tube length decreases fluid viscosity along the tube because viscosity decreases as the temperature increases. Decreasing viscosity results in increased particle motion, which may facilitate the formation of free convection. Therefore, this increase in the temperature

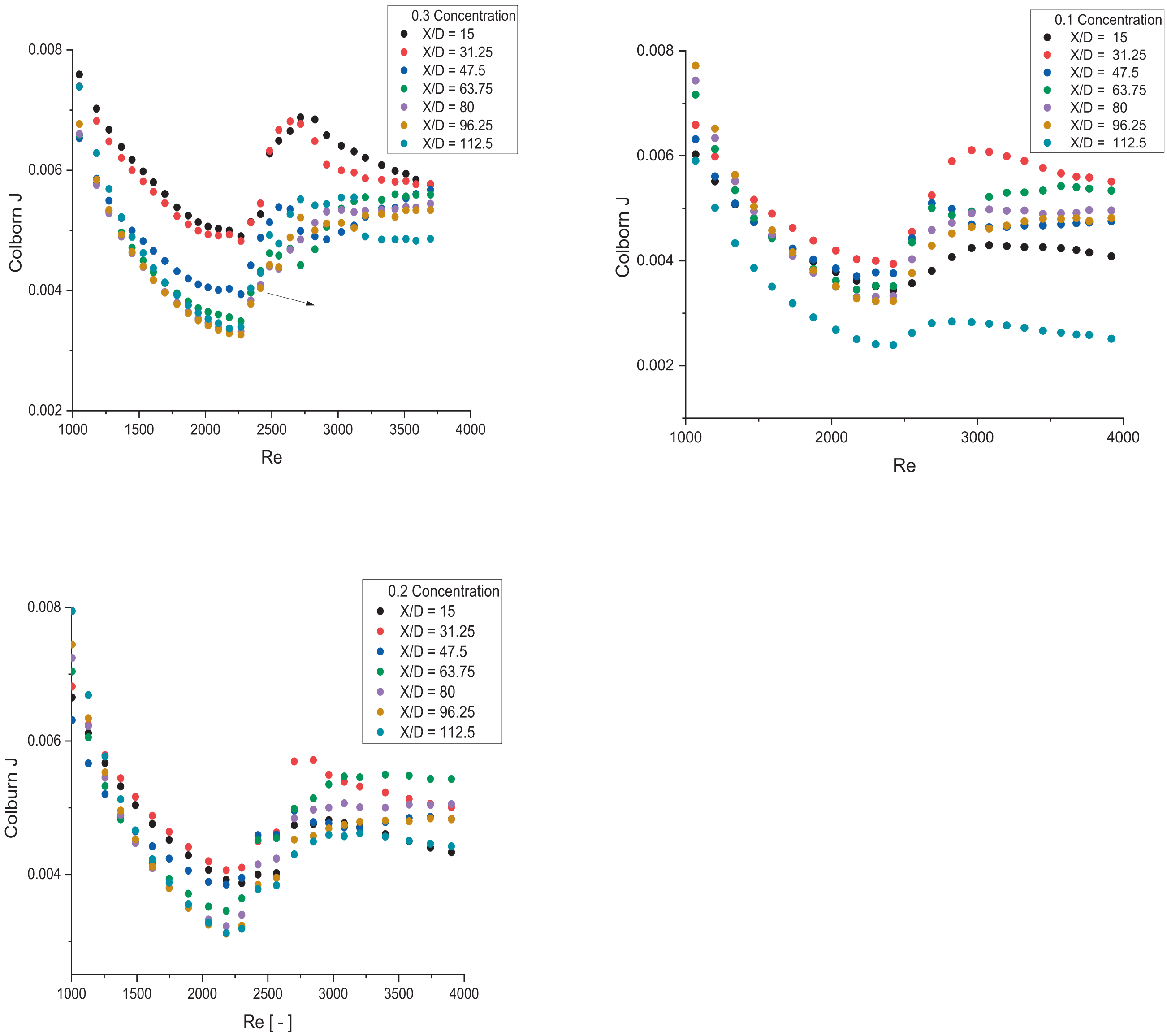

Fig. 8. Local Colburn J factor data against the Reynolds number.

gradient with the increase in X/D along the tube increased the fluid critical Reynolds number (i.e., transition lower limit). Ghajar and Tam [53] also explained that these transition limits are inlet dependent. Their findings show that the start and end of the transitions were varied with the use of different inlet configurations. It was also gathered that free convections dominate the flow over forced convection at the lower transition and laminar regions (i.e., depending on the tube and inlet configurations). The free convection effects have a significant impact on the lower transition and laminar regions. Together with the rise in the temperature gradient and reduction of the fluid viscosity, the critical Reynolds number increases along the tube as presented in Fig. 8. Research also indicates that it's not only the start of the transition that is affected, but also the transition width decreases from Fig. 8 (i.e., 0.3 vol concentrations).

However, one important point to be noted here is the influence of the axial position on this experiment. The effects of axial position appeared to be decreasing with the decrease in concentration. As the concentration decreases, the influence of fluid viscosity is reduced. Same with its effects on heat transfer, too. Concerning the end of the transition, some significant changes were noted for 0.3 % and 0.2 % volume concentration. However, for a 0.1 % volume concentration at X/D = 15, the end of the transition was at 2950, while at X/D = 112.5, the transition ends at 2700. The end of the transitions was harder to analyse for all the axial positions because of the scattered data points. Everts and Meyer also reported a similar situation [50] and attributed it to a lower temperature difference. The lower temperatures at the end of the transition also increase the uncertainties. This was also noticed to be reduced as the volume concentration decreased.

2.4. Heat transfers in the laminar and transition region

This part presents a general overview of the research results. That is without considering the influence of mixed convection and the thermal entrance effects. This was to have an idea of how these three-volume concentrations performed if those effects were not taken into consideration.

Fig. 9 shows a graph plot of the hybrid nanofluid Nusselt number against the Reynolds number for the three-volume concentration. The volume concentrations examined are 0.3 %, 0.2 %, and 0.1 % concentration. The results indicate that a 0.3 % concentration has improved the heat transfer performance better than the two lower concentrations of the same hybrid nanofluid (i.e., 0.2 % and 0.1 %). 0.1 vol concentration

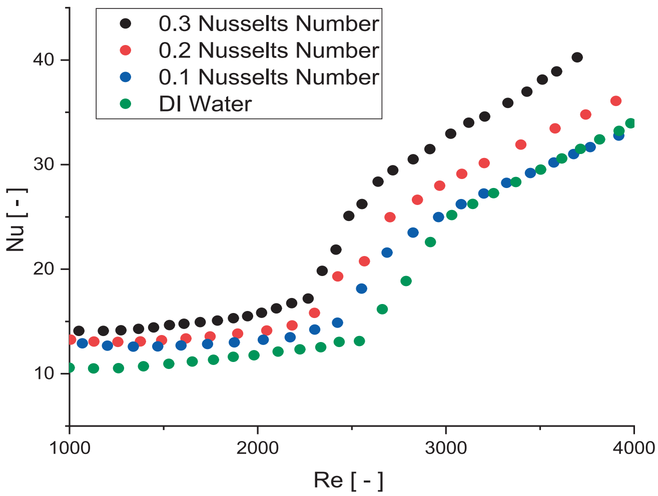

Fig. 9. Nusselt Number against the Reynolds Number.

has lower heat transfer performance than the 0.2 % volume concentration. These findings were in agreement with the findings of [37,57,58], where they all reported similar results. Fig. 2: The Hybrid nanofluid thermal conductivity value increases with the increase in the concentration. This important parameter also appeared to increase with temperature. The influence of volume concentration cannot only be attributed to thermal conductivity. Because the specific heat capacity of the fluid was also related to the fluid volume concentration, as shown in Eq. (4). The essence of adding these particles to the base fluid was based on the fact that these nanoparticles have better thermal conductivity than the base fluid. They were dispersed in the base fluid to harness these capabilities to form a nanofluid [7], giving them distinguished properties and characteristics that improve their heat transfer characteristics. Therefore, it's not surprising that thermophysical properties were varied with volume concentrations.

In this experiment, heat transfer performance with 0.3 % volume concentration, at a laminar Reynolds number of Re = 1350, has improved to about 8.3 % percent as compared to 0.2 % volume concentration. When comparing 0.3 % volume concentration to 0.1 % volume concentration, an improvement of about 12 % was recorded at the same Reynolds number.

A better-enhanced heat transfer was experienced in the transition region with all the volume concentrations. With a 0.3 % volume concentration, an improvement of about 21 % was recorded when compared to the 0.2 % at a transitional Reynolds number of 2550. This is much higher than the improvement recorded in the laminar region between the two concentrations. A similar enhancement was also noticed between 0.3 % and 0.1 % volume concentrations at the same Reynolds number of 2550 over the laminar region. A much higher improvement between the two concentrations was recorded compared to what we have noticed in the laminar regime. Because 0.3 % volume concentrations have an improvement of about 32 % compared to the 0.1 % in the transition region. 0.2 % volume concentration has also shown a remarkable heat transfer improvement in the transition. The Nusselt number value improved as compared to the 0.1 % volume concentration, which was raised to about 23 % higher than the 0.1 % volume concentration. However, along the turbulent regime, the Nusselt number improvement was reduced drastically compared to the transition regime. But it's still better than the laminar regime.

To understand the improvement in the heat transfer capabilities of this hybrid nanofluid of Al_2O_3 – MWCNT. Nanofluid experimental data were compared to the DI-water, the base fluid. This was to discover the impacts of dispersing these nanoparticles in the base fluid. Results indicate that dispersing these particles in DI water has remarkably improved in both regimes (i.e., laminar, transition, and turbulent). Especially with the higher volume concentration (i.e., 0.3 and 0.2). At Re = 3380 in the turbulent regime, a 0.3 % volume concentration has recorded a Nusselt number improvement of 24 %. In the transitional region, where the hybrid nanofluid has shown much better improvements than we discussed earlier, the improvement over water data was about 50 % at the transitional Reynolds number Re = 2550. While in the laminar regime at a Re = 1260, Nusselt was enhanced by 25.6 % compared to water. Similar findings were also noticed with a 0.2 concentration in all three regimes. It recorded an improvement over the water of about 11.2 %, 36.77 %, and 19.2 %, in turbulent, transitional, and laminar regimes, respectively. However, in the case of 0.1 % volume concentration, significant improvement was only recorded at the laminar and transitional regimes. There is an improvement in Nusselt number data compared to water, which has risen to about 27.6 % in the transition regime (Re = 2550), while in the laminar region (i.e., Re = 1260) it's Nusselt data was enhanced by about 17 %. However, in the turbulent region, the heat transfer characteristics of these volume concentrations appeared to have deteriorated. At some point around the turbulent Reynolds Number of 3700, the Nusselt number of 0.1 % concentration was even lower than that of water, with about 0.6 %. Osman et al. also reported a similar result [39], where lower-volume concentrations have very low improvement compared to water.

From Fig. 7, we discussed the start of the transition regimes for this hybrid nanofluid. It can be noticed that the laminar flow ranges of the three-volume concentration are given in Table 3.

2.5. Mixed convection heat transfer characteristics and effects of axial position

Figs. 10–12 show the plots of Ω against the Reynolds number at three axial tube positions (X/D = 15, 63.75, 96.25). From the plots, experimental data were compared to the Ω_F (i.e., Eq. (30). Yang et. al. [29] explained that the higher the values of the Ω in the above Eq. (30), the more significant the influence of the secondary flow is on the regime. This also indicates how Reynolds' number influenced this phenomenon. It is important to investigate the effects of this phenomenon with regard to the Reynolds number. It was noticed that important fluid properties like viscosity and density, etc., varied as the Reynolds number increased or decreased, and also fluid temperature varied with both increases and decreases in Reynolds and X/D distance. These factors or parameters affect the secondary flow. Their characteristics or behaviour are directly related to the secondary flow significance in the tube.

From Fig. 10. It was noticed that the secondary flow significance

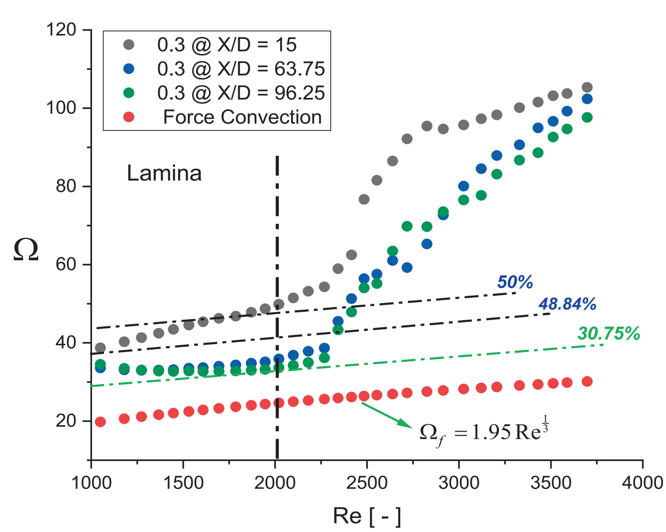

Fig. 10. Graphs of Ω and Ω_F against the Reynolds number at three different tube Axial distances of X/D = 15, 63.75 and 92.25 for 0.3 vol Concentration.

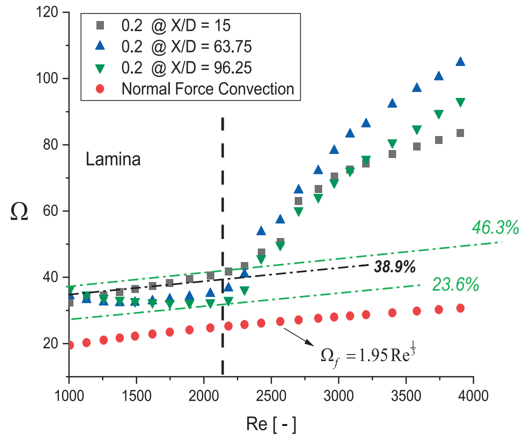

Fig. 11. Graphs Ω and Ω_F against the Reynolds number at three different Axial distances of X/D = 15, 63.75 and 92.25 for 0.2 vol concentration.

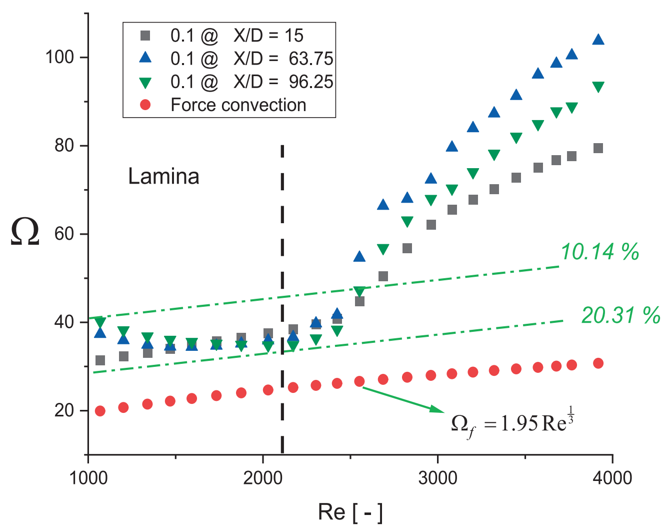

Fig. 12. Graphs of Ω and Ω_F against the Reynolds number at three different Axial distances of X/D = 15, 63.75 and 92.25 for 0.1 vol concentration.

reduces as the X/D position from the inlet increases. According to Eq. (30), for 0.3 vol concentration, at X/D = 15, the experimental data at a Reynold number of 1945 deviate from Eq. (30) (i.e.,) by 50 % while at the same Reynold number but at an X/D = 63.75, Ω and X/D = 96.25 values deviate from Ω_F by an approximate percentage of 38 %. However, what is uniquely different between these three axial positions is that, at X/D = 15, the Nusselt number appeared to increase with the increase of Reynolds. While at the axial positions of X/D = 63.75 and 96.25, this was not the case, as the Nusselt number appeared to have slightly decreased as the Reynolds number increased. This might likely be due to the entrance effects, which we will discuss later. Natural convection influences also show a greater strength at a lower Reynold number than at the higher Reynold number at the axial positions of X/D = 63.75 and 96.25. Because at Reynold's number of 1000, Ω deviates from the Ω_F by about 41 % and 42.6 % respectively, as compared to the values at Re = 1945 (i.e., where Ω and Ω_F only differ by about 38 %). This makes it even more obvious that axial position is significant concerning heat transfer characteristics.

Figs. 11 and 12 show the plots of the Ω and Ω_F for concentrations of 0.2 and 0.1. 0.3 vol concentration data at three axial positions were also considered, which are 15, 63.75, and 96.25. The results show that the effects of mixed convection are reduced with the decrease in volume concentration. That is when compared to Fig. 10, which presents the 0.3 vol concentration. For a 0.2 vol concentration, at a lower Reynolds number, mixed convection strengths were much stronger at X/D 63.75 and 96.25 than at X/D = 15. A deviation of Ω from Ω_F was about 43.23 % and 46.3 % at X/D = 63.75 and 96.25, respectively, as against the value at X/D = 15, which was only about 39.9 %. This shows that at a very low Reynolds number, mixed convection effects are increasing with the increase in the axial position. However, at a much higher Reynolds number, such as Re = 2000, mixed convection appeared to have decreased with the increase in the X/D distance from the inlet. With 0.2 vol concentration, Ω deviates from the Ω_F with an approximate percentage of 38.95 %, 29.42 % and 23.595 % for X/D = 15, 63.75 and 96.25 %, respectively.

A similar trend of results was also shown by 0.1 vol concentration, where mixed convection at a Reynolds number of Re = 2000 appeared to have decreased with increasing X/D distance from the inlet. At X/D = 15, 63.75 and 96.25, Ω differs from the Ω_F values with 12.86, 11.20 and 10.14 % respectively. This is a similar trend of results that were obtained with the other two concentrations (i.e., 0.3 and 0.2). Hybrid nanofluid mixed convection deteriorates along the tube length and also with the increase in the Reynolds number. Because even with 0.1 vol concentrations, the free convection effects were higher at Re = 1000 than at Re = 2000. At Re = 1000, Ω and Ω_F differ, with 17.43 and 20.311 % at X/D = 63.75 and 96.25, respectively. This indicates that the mixed convection's influence deteriorates with an increase in the Reynolds number and X/D from the inlet. The only exception is the X/D = 15, which differs by only 11.4 %. Similar results were also noticed with 0.3 and 0.2 at the same axial distance of X/D = 15, which we regarded as the results of the entrance effects. This is interesting because the results analysed for 0.3, 0.2, and 0.1 X/D = 15 behave similarly and are distinctive from the other two positions. This is because the entrance characteristics and their effect are the most significant at that position.

2.6. Thermal entrance effects on the mixed convection heat transfer

In this section, we will examine the results concerning the axial position x/d = 15, where the local Nusselt number appeared to have a slightly different trend of results (i.e., Fig. 13).

Entrance effects were believed to significantly influence the heat transfer behaviour of fluids in the developing regions. The thermal entrance region is the region where the thermal boundary layer is still developing (i.e., thermally developing flow). Fig. 14 shows a schematic diagram of the tube sections with the descriptive representations of the tube axial positions and the regions where distinctive characteristics were noticed in this research.

Mixed convection heat transfer conditions along the thermally developing region have not been investigated with nanofluids. But research in the area with other conventional fluids revealed some interesting findings. Example from the research work of Meyer et al. [48] identifies and defines these regions as forced convection developing and mixed convection developing regions. While Coetzee et al. [59] further classified these regions within the developing flow region as forced convection, free convection developing and sustained free convection. This shows the existence of a different and unique heat transfer characteristics that were experienced within the developing regions. But one thing that is common with all these findings is that; It was believed that the differences were as a result of developing thermal boundary layer. that is why in this research, we defined these regions as just thermal entrance and mixed convection regions. Thermal entrance was used to signify the region as that part of the tube where the thermal entrance effects were most significant. This was also supported by the findings of Shome et al. [9] and Everts et al. [26].

For sure, under forced convection conditions. Local Nusselt numbers reduce with an increase in X/D distance. This is due to very thin thermal boundary layer thicknesses, which are regarded as entrance effects [26]. Everts et al. [26] explained that thermal entrance increases as the Reynolds number increases; therefore, at a particular axial distance,

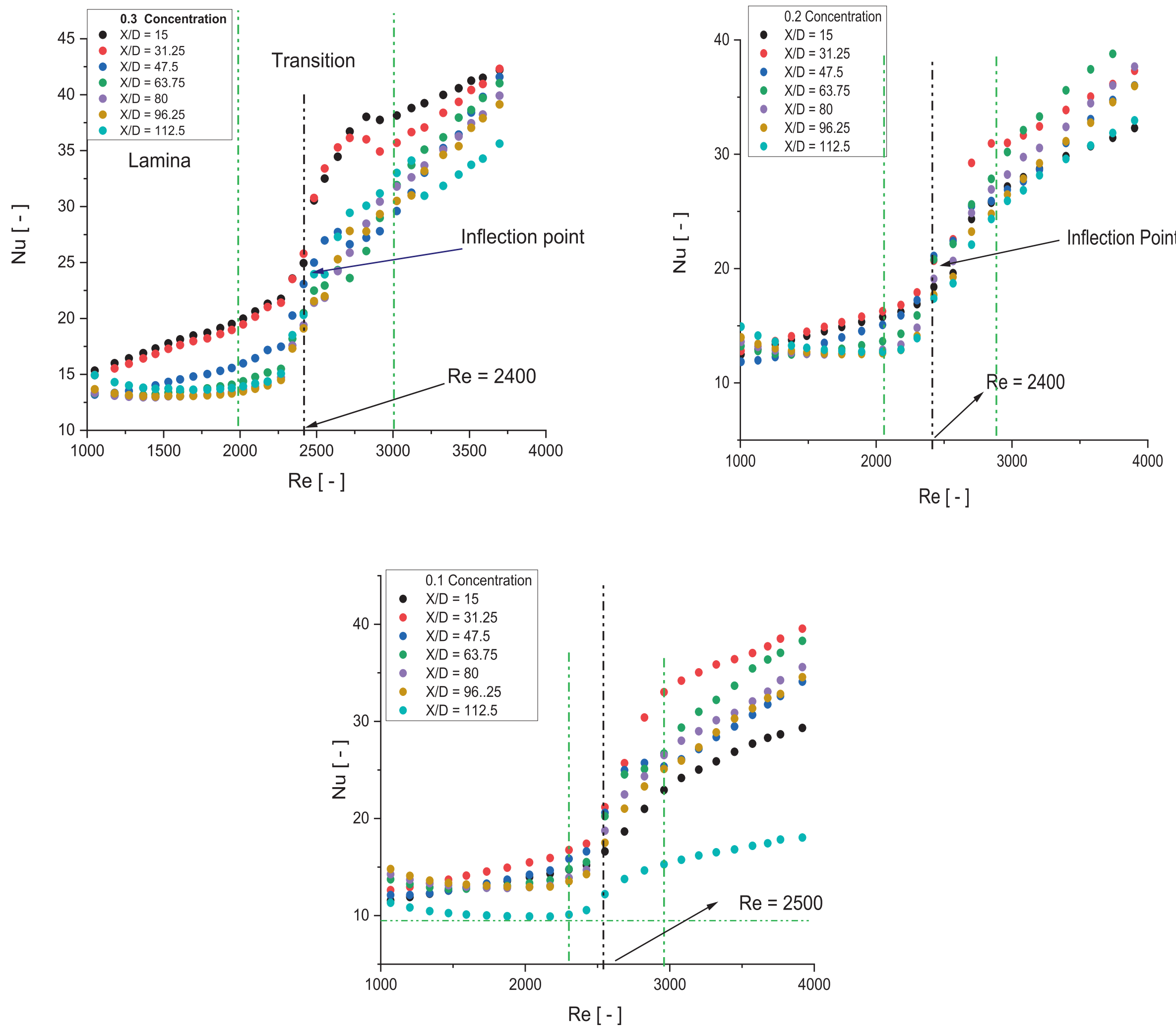

Fig. 13. Local Nusselt Number as a Function of Reynolds Number at Different Axial Positions.

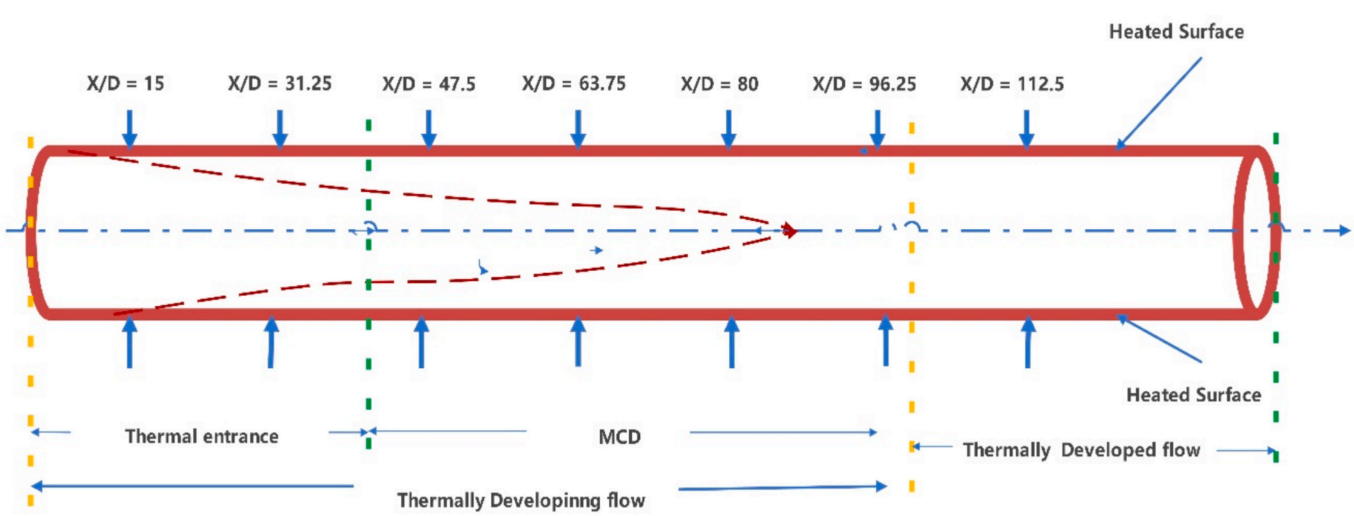

Fig. 14. Schematics diagram of the tube section.

thermal boundary layer thickness decreases, resulting in the Nusselt numbers' rise. Nusselt's number rise will continue as the Reynolds number increases at those axial positions (i.e., where entrance effects are significant). From Fig. 13a and 10, which presents the 0.3 concentration of the nanofluid, we can see that, at an axial distance of X/D = 15, Nusselt's number is increasing as the Reynolds number is increasing (i.e., from the Re = 1000 to Re = 2200). This indicates that the thermal boundary layer at X/D = 15 for the 0.3 vol concentration is very thin.

This resulted in an increase in the local Nusselt numbers compared to Reynolds's number. But at this point, it is important to stress that the deviation of Ω with Ω_F is not due to the mixed convection effects, but rather due to the entrance effects. It's the entrance effects that influence the rise in the Nusselt number. The possibility of mixed convection effects cannot be ruled out completely, but their effects are not as significant as the thermal entrance effects. Fig. 13 (b and c), Figs. 11, and 12 present the results of 0.2 and 0.1 vol concentrations, respectively. We notice that thermal entrance effects decrease with a decrease in the volume concentrations, but still appear to dominate the mixed convection effects at that particular axial position of X/D = 15. This was evident because the Nusselt number value rises with Reynolds' number [26].

It's very important to differentiate between the points where the mixed convection and entrance influences are the most dominant. To appropriately differentiate these two important regions, we adopt a method from the work of Everts et al. [26]. According to Everts et al. [26] , entrance effects are dominant if the gradient of the Nusselt number with respect to the Reynolds number is higher than zero. This was expressed in Eq. (42). and pictorially presented in Fig. 14.

$$\frac{dNu}{d\mathrm{Re}} > 0 \tag{42}$$

Fig. 15. It shows that at X/D = 15, Eq. (42) shows that entrance effects are the most dominant for the three concentrations over the mixed convection. Its effects enhance heat transfer (i.e., Nusselt Number). Because Shome et al. [9] stated that at an axial distance very close to the tube inlet, the increase in heat transfer was due to the entrance effects and viscosity, which agreed with our research findings.

Mixed convection effects dominate when the thickness of the boundary layer (i.e., Thermal boundary layer) develops significantly. The thermal boundary layer develops or increases across the tube length in the direction of the flow [47]. Its thickness increases as the X/D distance from the inlet increases. As the free convection effects start to dominate, the thermal entrance length decreases [26]. Therefore, the Nusselt number will decrease at a particular axial position as the Reynolds number increases. This is due to increased thermal boundary layer thickness (i.e., Entrance effects). However, with the development of free convection effects, which increase with the increase in thermal boundary layer thickness, the local Nusselt number will start increasing along the length of the tube as the free convection effects develop. This was normally regarded as the natural convection effects or free convection effects, as explained by Everts et al. [26] But in an event where the entrance effects are still more significant than the mixed convection, despite the development of the thermal boundary layer, the Nusselt number will decrease as the Reynolds number increases, and this is because of the shorter thermal entrance length. This may also be due to the influence of free convection or natural convection. Therefore, the condition given in Eq. (42) will prevail. If mixed convection influences are more significant than the entrance effects, the gradient of the Nusselt number becomes less than zero. This is presented in Eq. (43) and in Fig. 16.

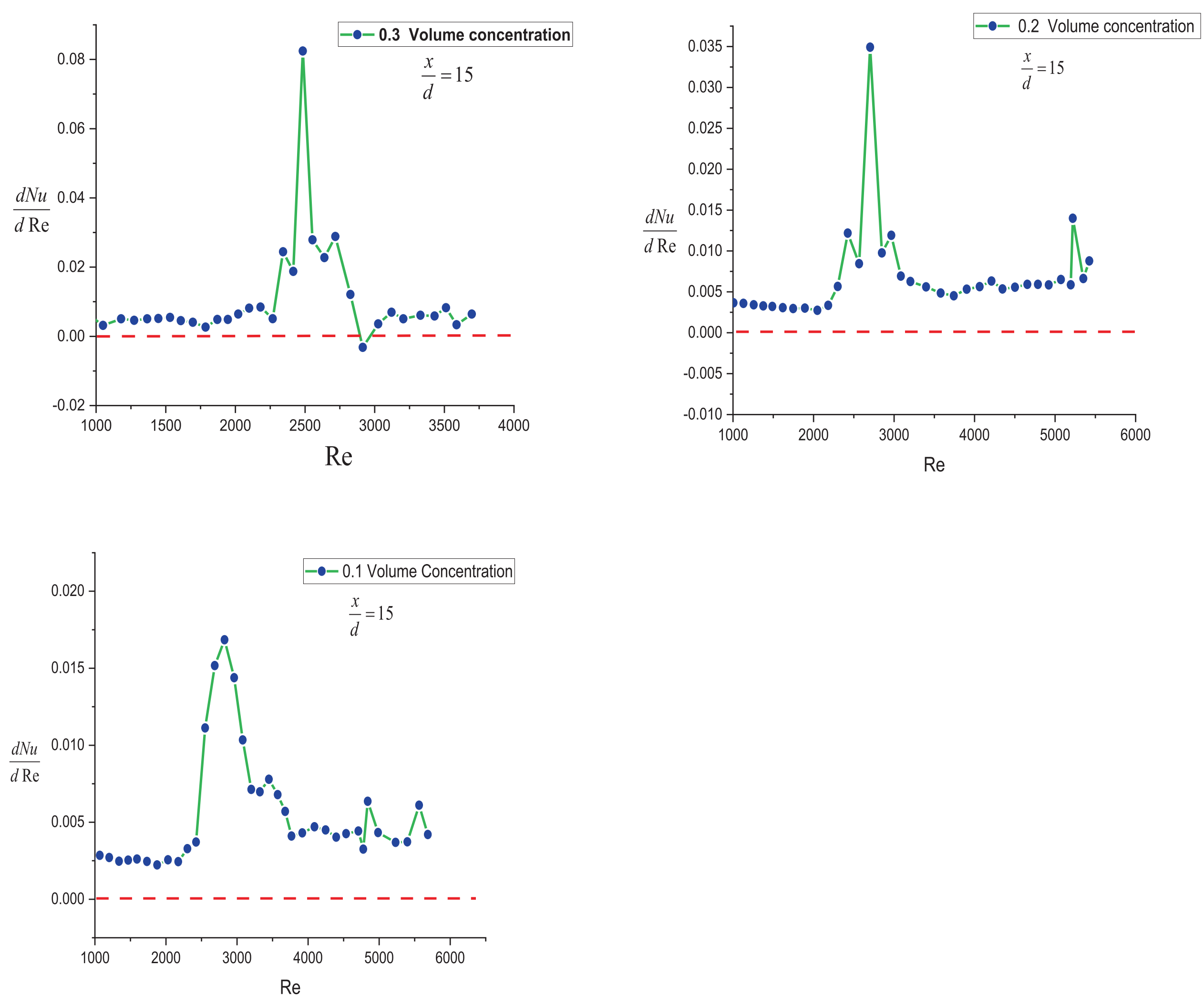

Fig. 15. Nusselt Number gradient against Reynold number at an Axial Position of X/D = 15.

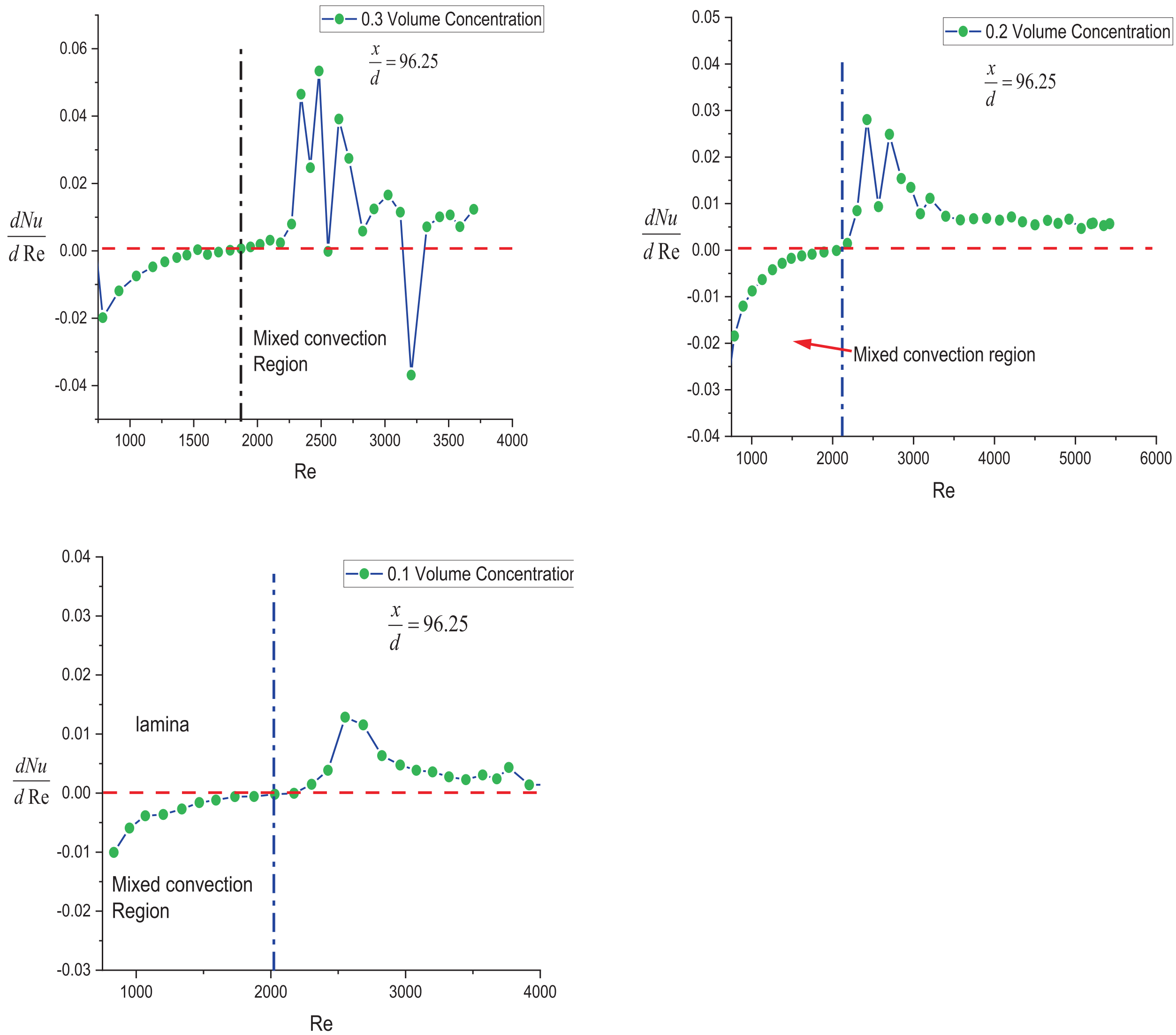

Fig. 16. Nusselt Number gradient against Reynolds' number at Axial distance of X/D = 96.25.

$$\frac{dNu}{d\mathrm{Re}} < 0 \tag{43}$$

In Fig. 16, the mixed convection condition was evident at the axial distance of X/D = 96.25. Unlike the other axial position, where entrance effects dominated the heat transfer as indicated in Fig. 15 (i.e., 0.3 Concentration). In Fig. 16, mixed convection appeared significant between the Reynolds number ranges of 1000 to 1900. While with 0.2 and 0.1 vol concentration, the influence of the mixed convection effects is very significant only between the Reynold numbers of 1000——2050 and 1000——1900, respectively. It is important to note that mixed convection effects may still likely be more significant at Reynolds numbers less than 1000, but in this research, our focus was only between 1000 and 4000.

2.7. Effects of volume concentration on mixed convection

We have already found that the positions in which the free convection effects are more significant in the laminar region are X/D = 63.75 and 96.25. Now we will try to analyse the impact of hybrid nanofluid volume concentration on heat transfer characteristics. This is important because, at a laminar region, the rate of flow is normally very slow, and also, depending on the heat flux, the radial temperature difference tends to be very high in this region. Radial temperature decreases with increasing Reynolds number. In an instant where the heat flux is very high, the radial temperature rises significantly across the tube length. This results in the development of thermal boundary layer thickness, and the fluid viscosity will be reduced accordingly. Because of this rise in temperature, the dispersed nanoparticles in the base fluid get excited, and particle motions within the fluid also increase. Fluids that are exposed to high temperatures will start to move, resulting in the formation of secondary flow effects.

Fig. 17 shows that the hybrid nanofluid's 0.3 and 0.2 vol concentrations have lower Nusselt numbers than 0.1. It is important to note that Fig. 17 shows Nusselt numbers plotted as a function of the dimensionless parameter called the Rayleigh number. Similar results were noticed at axial positions X/D = 63.75 and X/D = 96.25. The results of the two cases show that mixed convection effects are more significant in the lower concentration (i.e., 0.1 vol concentration). Similar results were reported in the experimental work of Mansour et al. [60] where volume concentration effects on the mixed convection heat transfer were investigated. The results show that, with an increase in volume concentration, natural convection influences are reduced. This is due to the increase in viscosity, which reduced or suppressed the buoyancy-

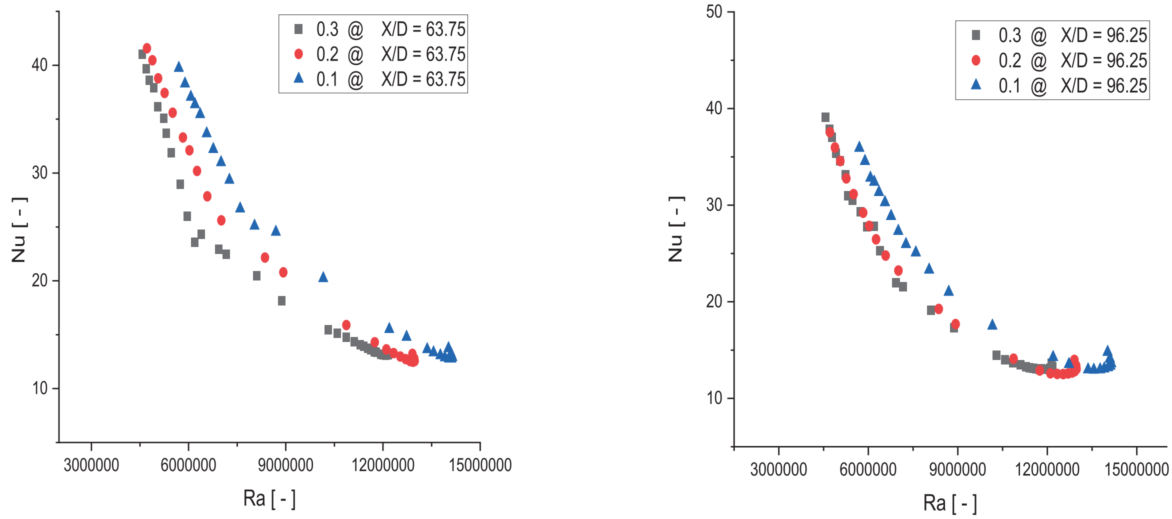

Fig. 17. Nusselt Numbers against the Raleigh number at two axial distances of X/D = 63.75 and 98.25, respectively.

induced secondary flow, even though the increase in radial temperature is the main cause of the mixed convection. However, viscosity and density change with the rise of temperature, affecting the intensity of the mixed convection. High viscosity and density reduce the buoyancy-induced secondary flow motion.

Fig. 17 shows that the Raleigh number increases with the decrease in Nusselt number at the two-axial position. The difference between the Raleigh number at the lower Nusselt number is not very significant. However, 0.1 concentration has shown the highest Raleigh number compared to the other two volume concentrations. This shows that mixed convection influences are very much stronger at lower concentrations. This should not be contradicted by higher heat transfer capacity. Despite having the highest influence of the mixed convection, 0.2 and 0.3 vol concentrations still have a much higher heat transfer capacity than 0.1(i.e., Fig. 9). At a laminar Reynolds' number of 1000, Raleigh's number of 0.3 vol concentration is less than that of 0.2 concentration by about 6.4 %. When 0.2 was compared with 0.1 vol concentration, 0.1 vol concentration was higher by 9.0 % at the axial position of 63.75. But this difference in Raleigh number reduces with an increase in tube position (i.e., from the tube inlet). Because at X/D = 96.25, and Reynold's number of 1000, Raleigh's number of 0.3 vol concentration differed by just 6.01 % from the 0.2 concentration. A similar reduction was noticed with 0.1 and 0.2 concentrations, as Raleigh's number of 0.1 vol concentrations was higher than that of 0.2 by 8.44 % as compared to the 9.0 % at the x/d = 63.75. This showcases the influence of the concentration of nanofluids on mixed convection heat transfer. To summarise the results, we can say that by increasing the nanofluid concentration from 0.1 to 0.3, the Raleigh number was reduced by about 18.0 % at X/D = 96.25.

As explained earlier, parameter ϕ, which was given in Eq. (28), signifies the natural convection influence. Feng et al. [44] explained that the higher the value of ϕ, the higher the influence of the mixed convection. Fig. 18 shows the plot of the ϕ against the product Grashof number, Prandtl number, and the ratio of the tube diameter to the length of the tube (Gr. Pr. $\frac{D}{L}$). The findings also reaffirmed the earlier findings from Fig. 17 using the Raleigh number. It shows that an increase in the volume concentration has deteriorated the influence of free convection. 0.1 vol concentration has experienced a much higher free convection influence. In other words, buoyance-induced secondary flow is much more significant with 0.1 vol concentration than with 0.2 and 0.3. However, this influence is reduced with an increase in tube length. These findings agreed with the work of Mansour et al. [60] and Li et al. [7] and this was not only among the laminar region but also in the transition and turbulent regimes Fig. 18.

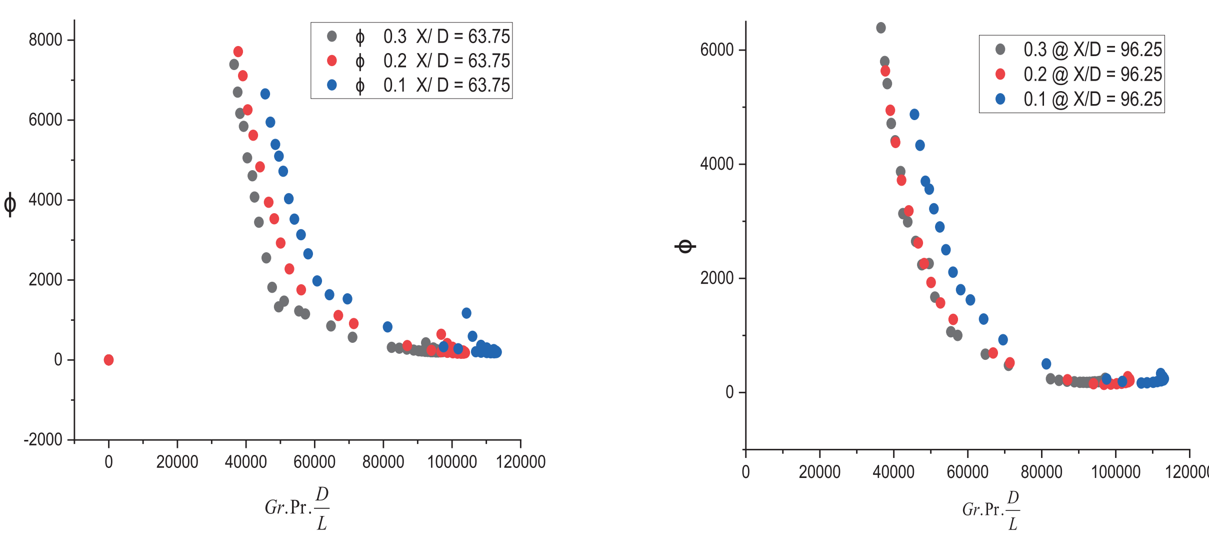

Fig. 18. Plot of ϕ against Gr. Pr. $\frac{D}{L}$ at two axial distances of X/D = 63.75 and 98.25, respectively.

2.8. Mixed convection in the transition and turbulent region

Due to the specific nature and characteristics of the transition region, we decided to analyse its mixed convection heat transfer in terms of another dimensionless parameter called the Richardson Number (Ri). The Richardson number can be used to appropriately quantify mixed convection in all three flow regimes. Cengal et al. [47] and Evert et al. [61] stated that when the Richardson number is less than 0.1, the flow will likely be under forced convection. However, if it is greater than 10, it is assumed that the entire flow was overwhelmed by secondary flow. However, when the Richardson number ranges from 0.1 to 10, the flow is expected to be under mixed convection. From this, we can see that the method used to analyse the laminar data is on point. From Fig. 19, all the laminar data fall within the mixed convection area under the two axial conditions. This added a level of confidence in our previous analysis. Also, in the same vein, when we compare Fig. 18, we analyse the effects of volume concentration. Fig. 19 shows that mixed convection effects are much higher with 0.1 vol concentration. From Fig. 19, it has become clearer that 0.3 was the least in terms of forced convection. It also shows that high viscosity suppressed the buoyancy-induced secondary flow, which results in the reduction of mixed convection influence. This can be seen from the two axial positions as presented in Fig. 19. While in Fig. 18, it can only be noticed at X/D = 63.75. Fig. 19 shows that all the transition data fall within the range of 0.1 to 10. This signifies that mixed convection existed in the transition region. It was also noticed that the mixed convection influence reduced with the increasing Reynolds number from laminar to transition and then to turbulent. It can also be seen that the turbulent data were all below the 0.1 boundaries. This indicates that, in these experiments, forced convection dominated the turbulent flow region. Therefore, the region can be regarded as a pure forced convection region.

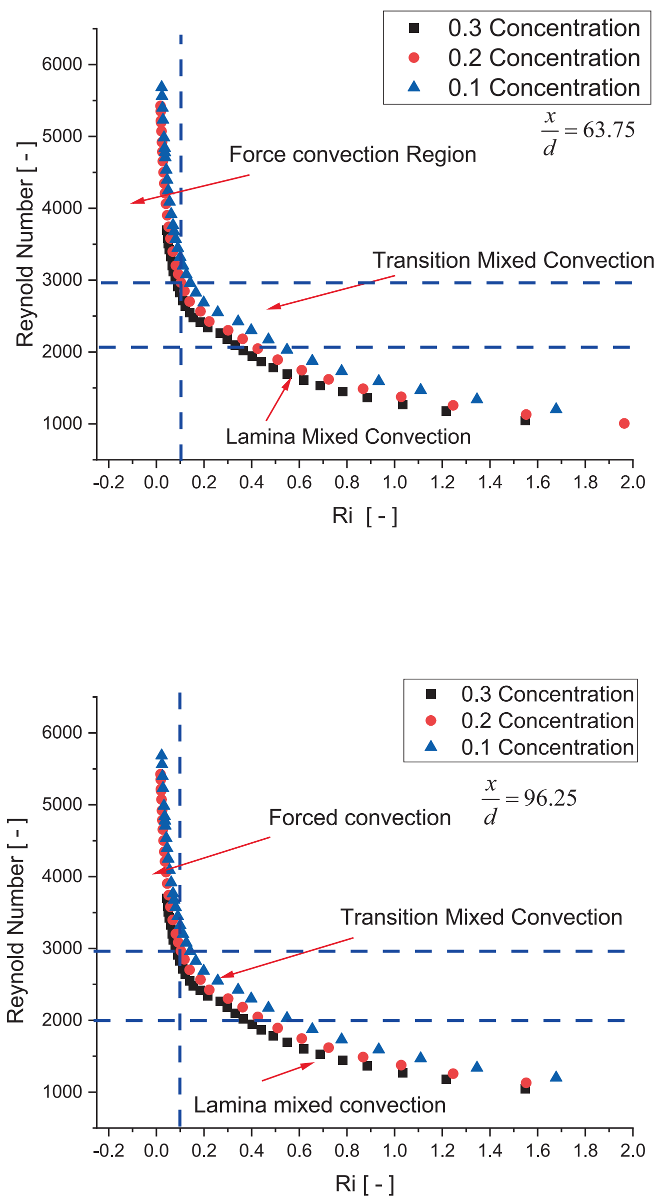

Fig. 19. Reynolds number against Richardson Number at two axial distances of X/D = 63.75 and 98.25, respectively.

3. Conclusion

In this research study, a hybrid nanofluid of Al_2O_3 (60 %) – MWCNT (40 %) is prepared and evaluated under constant heat flux conditions. Three volume concentrations of 0.3, 0.2, and 0.1 were used. From the experimental data analyzed, the following summarized conclusions were made.

- From the experimental results, we found that an increase in volume concentration results in varying the fluid heat transfer characteristics, which also affects the flow boundaries. Results show that the critical Reynolds numbers of the three-volume concentration differ. This means that the start of the transition regime differs as the volume concentration varies. It shows that the critical Reynolds number decreases with increased volume concentration. Volume concentrations were also found to affect the end of the transition flow. This affects the range of the transitional regime. This signifies that the range of laminar, transition and turbulent regions depends on the volume concentration.
- The hybrid nanofluid heat transfer behaviours also varied with an increase in X/D distance from the tube inlet. Research findings show that this was due to the effects of the thermal entrance region, and it holds true for all volume concentrations and throughout all three regimes.
- This experiment found the highest heat transfer enhancement in the transition region, with 0.3 vol concentration, followed by 0.2 and 0.1. At a transitional Reynolds number of 2550, a 0.3 concentration has an enhancement of about 21 % compared to a 0.2 concentration. Meanwhile, it is better than 0.2 concentration in the laminar region by 8.3 %. This shows there are much better enhancements in the Nusselt number at the transition region than in the laminar and turbulent regions.
- Compared to the base fluid, Nanofluids have shown better heat transfer than the base fluid at both regions. 0.3 concentration has the highest increase in Nusselt number over the base fluid, especially in the transition region, where it has an enhancement of about 50 % compared to the base fluid.
- These research results indicate that Eqs. (34) and (35) precisely characterise and identify the boundaries of these hybrid nanofluids. These equations distinguish the entrance and region where mixed convection effects are the most dominant. These results are incredibly significant, especially in analytical and numerical studies of these hybrid nanofluids.
- Mixed convection effects were found to be more important within the laminar regime than in the transition and turbulent regimes. Mixed convection effects were also found to decrease with increasing Reynolds number, axial position, and Volume concentration.
- Hybrid nanofluid heat transfer characteristics in the entrance region were found to be different from those in the developing region. The thermal entrance was also found to be decreasing with decreasing volume concentration. While the Nusselt number in the region increased with an increase in Reynolds' number.

- Unlike Mixed convection effects, thermal entrance effects extend to both transition and turbulent regions. However, its influences decrease drastically with the decrease in volume concentration.
- Richardson numbers were found to increase with the decrease in volume concentration. This signifies that the contribution of heat transfer enhancement with respect to free convection is higher than the contribution due to forced convection with low volume concentration (i.e., in 0.1 concentration).

CRediT authorship contribution statement

Ibrahim Umar Ibrahim: Writing – original draft, Visualization, Validation, Methodology, Investigation, Formal analysis, Data curation, Conceptualization. **Mohsen Sharifpur:** Writing – review & editing, Validation, Supervision, Resources, Project administration, Methodology, Funding acquisition. **Josua P. Meyer:** Writing – review & editing, Supervision, Resources, Project administration, Methodology, Funding acquisition.

Declaration of competing interest

The authors declare that they have no known competing financial interests or personal relationships that could have appeared to influence the work reported in this paper.

Data availability

Data will be made available on request.

References

[1] S.O. Giwa, M. Momin, C.N. Nwaokocha, M. Sharifpur, J.P. Meyer, Influence of nanoparticles size, per cent mass ratio, and temperature on the thermal properties of water-based MgO–ZnO nanofluid: an experimental approach, J. Therm. Anal. Calorim. 143 (2) (2021) 1063–1079, https://doi.org/10.1007/S10973-020-09870-X/FIGURES/23.
[2] M.H. Ahmadi, A. Mirlohi, M. Alhuyi Nazari, R. Ghasempour, A review of thermal conductivity of various nanofluids, J. Mol. Liq. 265 (2018) 181–188, https://doi.org/10.1016/j.molliq.2018.05.124.
[3] J. Buongiorno, Convective transport in nanofluids, J. Heat Transfer 128 (3) (2006) 240–250, https://doi.org/10.1115/1.2150834.
[4] M. Yasuo, F. Kozo, T. Shinobu, N. Masakuni, Forced convective heat transfer in uniformly heated horizontal tubes 1st report—experimental study on the effect of buoyancy, Int. J. Heat Mass Transf. 9 (5) (1966) 453–463, https://doi.org/10.1016/0017-9310(66)90101-3.
[5] Y.S. Chen, H.H. Zhu, J. Tian, Y. Fu, Z.F. Tang, N.X. Wang, Convective heat transfer characteristics in the laminar and transition region of molten salt in concentric tube, Appl. Therm. Eng. 117 (2017) 682–688, https://doi.org/10.1016/J.APPLTHERMALENG.2017.01.070.
[6] D.R. Oliver, The effect of natural convection on viscous-flow heat transfer in horizontal tubes, Chem. Eng. Sci. 17 (5) (1962) 335–350, https://doi.org/10.1016/0009-2509(62)80035-9.
[7] W. Li, Z.Z. Feng, Laminar mixed convection of large-Prandtl-number in-tube nanofluid flow, Part II: correlations, Int. J. Heat Mass Transf. 65 (2013) 928–935, https://doi.org/10.1016/J.IJHEATMASSTRANSFER.2013.07.006.
[8] A. E. Bergles, Experimental verification of analyses and correlation of the effects of temperature-dependent fluid properties on laminar heat transfers., pp. 473–486, 1983.
[9] B. Shome, M.K. Jensen, Mixed convection laminar flow and heat transfer of liquids in isothermal horizontal circular ducts, Int. J. Heat Mass Transf. 38 (11) (1995) 1945–1956, https://doi.org/10.1016/0017-9310(94)00328-S.
[10] R. Ben Mansour, N. Galanis, and C. T. Nguyen, Developing laminar mixed convection of nanofluids in an inclined tube with uniform wall heat flux, Int. J. Numer. Methods Heat Fluid Flow, 19(2) (2009), pp. 146–164, Doi: 10.1108/09615530910930946/FULL/PDF.
[11] M. Akbari, A. Behzadmehr, F. Shahraki, Fully developed mixed convection in horizontal and inclined tubes with uniform heat flux using nanofluid, Int. J. Heat Fluid Flow 29 (2) (2008) 545–556, https://doi.org/10.1016/J.IJHEATFLUIDFLOW.2007.11.006.
[12] M.M. Derakhshan, M.A. Akhavan-Behabadi, Mixed convection of MWCNT–heat transfer oil nanofluid inside inclined plain and microfin tubes under laminar assisted flow, Int. J. Therm. Sci. 99 (2016) 1–8, https://doi.org/10.1016/J.IJTHERMALSCI.2015.07.025.
[13] N. Putra, W. Roetzel, S.K. Das, Natural convection of nano-fluids, Heat Mass Transfer/waerme- Und Stoffuebertragung 39 (8–9) (2003) 775–784, https://doi.org/10.1007/S00231-002-0382-Z/FIGURES/15.
[14] D. Wen, Y. Ding, Formulation of nanofluids for natural convective heat transfer applications, Int. J. Heat Fluid Flow 26 (6) (2005) 855–864, https://doi.org/10.1016/J.IJHEATFLUIDFLOW.2005.10.005.
[15] A.J. Ghajar, K.F. Madon, Pressure drop measurements in the transition region for a circular tube with three different inlet configurations, Exp. Therm Fluid Sci. 5 (1) (1992) 129–135, https://doi.org/10.1016/0894-1777(92)90062-A.
[16] R.M. Manglik, A.E. Bergles, Heat transfer and pressure drop correlations for twisted-tape inserts in isothermal tubes: Part II—transition and turbulent flows, J. Heat Transfer 115 (4) (1993) 890–896, https://doi.org/10.1115/1.2911384.
[17] J.G. Withers, Tube-side heat transfer and pressure drop for tubes having helical internal ridging with turbulent/transitional flow of single-phase fluid. Part 1. Single-Helix ridging, Heat Transfer Eng. 2 (1) (1980) 48–58, https://doi.org/10.1080/01457638008962750.
[18] T.C. Carnavos, Heat transfer performance of internally finned tubes in turbulent flow, Heat Transfer Eng. 1 (4) (1980) 32–37, https://doi.org/10.1080/01457638008939566.
[19] N.T. Obot, E.B. Esen, T.J. Rabas, The role of transition in determining friction and heat transfer in smooth and rough passages, Int. J. Heat Mass Transf. 33 (10) (1990) 2133–2143, https://doi.org/10.1016/0017-9310(90)90115-B.
[20] H.R. Nagendra, Interaction of free and forced convection in horizontal tubes in the transition regime, J. Fluid Mech. 57 (2) (1973) 269–288, https://doi.org/10.1017/S0022112073001151.
[21] M. Everts, J.P. Meyer, Relationship between pressure drop and heat transfer of developing and fully developed flow in smooth horizontal circular tubes in the laminar, transitional, quasi-turbulent and turbulent flow regimes, Int. J. Heat Mass Transf. 117 (2018) 1231–1250, https://doi.org/10.1016/j.ijheatmasstransfer.2017.10.072.
[22] H. Zontul, H. Hamzah, N. Kurtulmuş, B. Şahin, Investigation of convective heat transfer and flow hydrodynamics in rectangular grooved channels, Int. Commun. Heat Mass Transfer 126 (2021) 105366, https://doi.org/10.1016/J.ICHEATMASSTRANSFER.2021.105366.
[23] N. Tokgoz, M.M. Aksoy, B. Sahin, Investigation of flow characteristics and heat transfer enhancement of corrugated duct geometries, Appl. Therm. Eng. 118 (2017) 518–530, https://doi.org/10.1016/J.APPLTHERMALENG.2017.03.013.
[24] I.U. Ibrahim, M. Sharifpur, J.P. Meyer, S.M.S. Murshed, Experimental investigations of effects of nanoparticle size on force convective heat transfer characteristics of Al_2O_3 - MWCNT hybrid nanofluids in transitional flow regime, Int. J. Heat Mass Transf. 228 (2024) 125597, https://doi.org/10.1016/J.IJHEATMASSTRANSFER.2024.125597.
[25] I. Umar Ibrahim, M. Sharifpur, and J. P. Meyer, "Mixed Convection Heat Transfer Characteristics of Al2O3 – MWCNT Hybrid Nanofluid under Thermally Developing Flow; Effects of Particles Percentage Weight Composition," Appl Therm Eng, 249 (2024), p. 123372, Doi: 10.1016/J.APPLTHERMALENG.2024.123372.
[26] M. Everts, J.P. Meyer, Heat transfer of developing and fully developed flow in smooth horizontal tubes in the transitional flow regime, Int. J. Heat Mass Transf. 117 (2018) 1331–1351, https://doi.org/10.1016/J.IJHEATMASSTRANSFER.2017.10.071.
[27] S.M.S. Murshed, K.C. Leong, C. Yang, Investigations of thermal conductivity and viscosity of nanofluids, Int. J. Therm. Sci. 47 (2008) 560–568, https://doi.org/10.1016/j.ijthermalsci.2007.05.004.
[28] S.M.S. Murshed, K.C. Leong, C. Yang, Thermophysical and electrokinetic properties of nanofluids – a critical review, Appl. Therm. Eng. 28 (17–18) (2008) 2109–2125, https://doi.org/10.1016/J.APPLTHERMALENG.2008.01.005.
[29] Y. Yang, Z.G. Zhang, E.A. Grulke, W.B. Anderson, G. Wu, Heat transfer properties of nanoparticle-in-fluid dispersions (nanofluids) in laminar flow, Int. J. Heat Mass Transf. 48 (6) (2005) 1107–1116, https://doi.org/10.1016/J.IJHEATMASSTRANSFER.2004.09.038.
[30] K.B. Anoop, T. Sundararajan, S.K. Das, Effect of particle size on the convective heat transfer in nanofluid in the developing region, Int. J. Heat Mass Transf. 52 (9–10) (2009) 2189–2195, https://doi.org/10.1016/j.ijheatmasstransfer.2007.11.063.
[31] A. Ahmadi Nadooshan, H. Eshgarf, and M. Afrand, Measuring the viscosity of Fe3O4-MWCNTs/EG hybrid nanofluid for evaluation of thermal efficiency: Newtonian and non-Newtonian behavior, J. Mol. Liq., 253, pp. 169–177, 2018. doi: 10.1016/J.MOLLIQ.2018.01.012.
[32] S. Osman, M. Sharifpur, J.P. Meyer, Experimental investigation of convection heat transfer in the transition flow regime of aluminium oxide-water nanofluids in a rectangular channel, Int. J. Heat Mass Transf. 133 (2019) 895–902, https://doi.org/10.1016/j.ijheatmasstransfer.2018.12.169.
[33] S. O. Giwa, M. Sharifpur, M. H. Ahmadi, S. M. Sohel Murshed, and J. P. Meyer, Experimental Investigation on Stability, Viscosity, and Electrical Conductivity of Water-Based Hybrid Nanofluid of MWCNT-Fe2O3, Nanomaterials 2021, 11 (1) (2021) 136, doi: 10.3390/NANO11010136.
[34] S.O. Giwa, M. Sharifpur, J.P. Meyer, S. Wongwises, O. Mahian, Experimental measurement of viscosity and electrical conductivity of water-based γ-Al_2O_3/MWCNT hybrid nanofluids with various particle mass ratios, J. Therm. Anal. Calorim. 143 (2) (2021) 1037–1050, https://doi.org/10.1007/s10973-020-10041-1.
[35] I.U. Ibrahim, M. Sharifpur, J.P. Meyer, Experimental investigations of particle sizes effects on exergy and entropy characteristics of AL_2O_3 - MWCNT hybrid nanofluid along the transitional flow regime, Case Stud. Therm. Eng. 51 (2023) 103575, https://doi.org/10.1016/J.CSITE.2023.103575.
[36] L.S. Sundar, M.K. Singh, A.C.M. Sousa, Enhanced heat transfer and friction factor of MWCNT-Fe_3O_4/water hybrid nanofluids, Int. Commun. Heat Mass Transfer 52 (2014) 73–83, https://doi.org/10.1016/j.icheatmasstransfer.2014.01.012.
[37] M.T. Naik, L.S. Sundar, Heat transfer and friction factor with water/propylene glycol-based CuO nanofluid in circular tube with helical inserts under transition

flow regime, Heat Transfer Eng. 35 (1) (2014) 53–62, https://doi.org/10.1080/01457632.2013.810451.
[38] S. Suseel Jai Krishnan, M. Momin, C. Nwaokocha, M. Sharifpur, and J. P. Meyer, "An empirical study on the persuasive particle size effects over the multi-physical properties of monophase MWCNT-Al2O3 hybridized nanofluids," J Mol Liq, 361 (2022) doi: 10.1016/j.molliq.2022.119668.
[39] F. Durst, S. Ray, B. Ünsal, O.A. Bayoumi, The development lengths of laminar pipe and channel flows, J. Fluids Eng., Trans. ASME 127 (6) (2005) 1154–1160, https://doi.org/10.1115/1.2063088.
[40] J.P. Meyer, T.J. McKrell, K. Grote, The influence of multi-walled carbon nanotubes on single-phase heat transfer and pressure drop characteristics in the transitional flow regime of smooth tubes, Int. J. Heat Mass Transf. 58 (1–2) (2013) 597–609, https://doi.org/10.1016/j.ijheatmasstransfer.2012.11.074.
[41] S.I. Abu-Eishah, Correlations for the thermal conductivity of metals as, Int. J. Thermophys. 22 (6) (2001) 1855–1868.
[42] C.O. Popiel, J. Wojtkowiak, Simple formulas for thermophysical properties of liquid water for heat transfer calculations (from 0°c to 150°c), Heat Transfer Eng. 19 (3) (1998) 87–101, https://doi.org/10.1080/01457639808939929.
[43] B. Choon Pak and Y. I. Cho, Experimental heat transfer an international journal hydrodynamic and heat transfer study of dispersed fluids with submicron metallic oxide particles, (2007). doi: 10.1080/08916159808946559.
[44] Z.Z. Feng, W. Li, Laminar mixed convection of large-Prandtl-number in-tube nanofluid flow, Part I: experimental study, Int. J. Heat Mass Transf. 65 (2013) 919–927, https://doi.org/10.1016/J.IJHEATMASSTRANSFER.2013.07.005.
[45] C.A. Depew, S.E. August, Heat transfer due to combined free and forced convection in a horizontal and isothermal tube, J. Heat Transfer 93 (4) (1971) 380–384, https://doi.org/10.1115/1.3449834.
[46] A.R. Brown, M.A. Thomas, Combined free and forced convection heat transfer for laminar flow in horizontal tubes, J. Mech. Eng. Sci. 7 (4) (1965) 440–448, https://doi.org/10.1243/JMES_JOUR_1965_007_066_02.
[47] A. J. G. Yunus A. Cengal, Heat and Mass Trasnfer: Fundametals and Applications, Heat and Mass Trasnfer: Fundametals and Applications, vol. 1, pp. 67–142, 379–424, 2014, Accessed: Jun. 09, 2023. [Online]. Available: https://books.google.com/books/about/Heat_and_Mass_Transfer_Fundamentals_and.html?id=B89MnwEACAAJ.
[48] J.P. Meyer, M. Everts, Single-phase mixed convection of developing and fully developed flow in smooth horizontal circular tubes in the laminar and transitional flow regimes, Int. J. Heat Mass Transf. 117 (2018) 1251–1273, https://doi.org/10.1016/J.IJHEATMASSTRANSFER.2017.10.070.
[49] P. Dunn and M. Davis, Measurement and data analysis for engineering and science. 2017. Accessed: Oct. 07, 2023. [Online]. Available: https://books.google.com/books?hl=en&lr=&id=bmlQDwAAQBAJ&oi=fnd&pg=PP1&ots=H0LAUUIWz2&sig=Mi44eXrMD0KQ0w6qWH3ns-48R7o.
[50] J.P. Meyer, S.M. Abolarin, Heat transfer and pressure drop in the transitional flow regime for a smooth circular tube with twisted tape inserts and a square-edged inlet, Int. J. Heat Mass Transf. 117 (2018) 11–29, https://doi.org/10.1016/J.IJHEATMASSTRANSFER.2017.09.103.
[51] A.J. Ghmar, D.T. Strickland, Forced and mixed convective heat transfer correlations in the laminar-transition-turbulent regions for a circular tube y ith a square-edged entrance, AIAA/ASME 5th Joint Thermophysics and Heat Transfer Conference (1990.), https://doi.org/10.2514/6.1990-1762.
[52] F. Andrade, A.S. Moita, A. Nikulin, A.L.N. Moreira, H. Santos, Experimental investigation on heat transfer and pressure drop of internal flow in corrugated tubes, Int. J. Heat Mass Transf. 140 (2019) 940–955, https://doi.org/10.1016/J.IJHEATMASSTRANSFER.2019.06.025.
[53] A. J. Ghajar and L.-M. Tam, "Heat Transfer Measurements and Correlations in the Transition Region for a Circular Tube with Three Different Inlet Configurations," 1994.
[54] S. Zhang, Mixed convective heat transfer of medium-Prandtl-number fluids in horizontal circular tubes, Int. J. Heat Mass Transf. 190 (2022) 122740, https://doi.org/10.1016/J.IJHEATMASSTRANSFER.2022.122740.
[55] J. P. Abraham, E. M. Sparrow, and W. J. Minkowycz, Internal-flow Nusselt numbers for the low-Reynolds-number end of the laminar-to-turbulent transition regime. doi: 10.1016/j.ijheatmasstransfer.2010.09.012.
[56] E.N. Sieder, G.E. Tate, Heat transfer and pressure drop of liquids in tubes, Ind. Eng. Chem. 28 (12) (1936) 1429–1435, https://doi.org/10.1021/IE50324A027.
[57] K.V. Sharma, L.S. Sundar, P.K. Sarma, Estimation of heat transfer coefficient and friction factor in the transition flow with low volume concentration of Al2O3 nanofluid flowing in a circular tube and with twisted tape insert, Int. Commun. Heat Mass Transfer 36 (5) (2009) 503–507, https://doi.org/10.1016/j.icheatmasstransfer.2009.02.011.
[58] S.S. Chougule, S.K. Sahu, Comparative study on heat transfer enhancement of low volume concentration of Al_2O_3-water and carbon nano-tube-water nano-fluids in transition regime using helical screw tape inserts, Exp. Heat Transfer 29 (1) (2016) 17–36, https://doi.org/10.1080/08916152.2014.926432.
[59] M.J. Coetzee, D. Steyn, M. Everts, The local heat transfer characteristics associated with mixed convective developing flow through a horizontal tube exposed to a uniform wall temperature boundary condition, Int. J. Therm. Sci. 203 (2024) 109167, https://doi.org/10.1016/J.IJTHERMALSCI.2024.109167.
[60] R. Ben Mansour, N. Galanis, and C. T. Nguyen, Experimental study of mixed convection with water–Al_2O_3 nanofluid in inclined tube with uniform wall heat flux, Int. J. Therm. Sci., 50(3) (2011) pp. 403–410 Doi: 10.1016/J.IJTHERMALSCI.2010.03.016.
[61] M. Everts and J. P. Meyer, "Flow Regime Maps for Fully Developed Flow in Horizontal Solar Receiver Tubes".